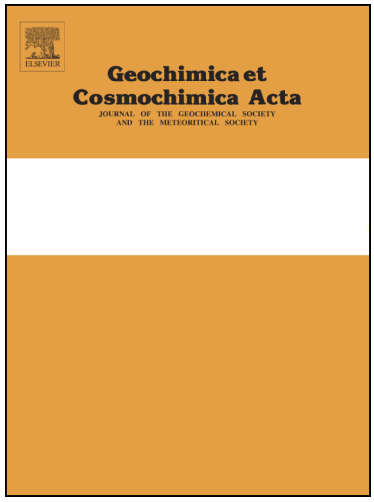

Coupled sulfur and oxygen isotope insight into bacterial sulfate reduction in the natural environment

Gilad Antler, Alexandra V. Turchyn, Victoria Rennie, Barak Herut, Orit Sivan

PII: S0016-7037(13)00269-X
DOI: http://dx.doi.org/10.1016/j.gca.2013.05.005
Reference: GCA 8261

To appear in: *Geochimica et Cosmochimica Acta*

Received Date: 18 October 2012
Accepted Date: 3 May 2013

Please cite this article as: Antler, G., Turchyn, A.V., Rennie, V., Herut, B., Sivan, O., Coupled sulfur and oxygen isotope insight into bacterial sulfate reduction in the natural environment, *Geochimica et Cosmochimica Acta* (2013), doi: http://dx.doi.org/10.1016/j.gca.2013.05.005

Coupled sulfur and oxygen isotope insight into bacterial sulfate reduction in the natural environment

Gilad Antler[1], Alexandra V. Turchyn[2], Victoria Rennie[2], Barak Herut[3], Orit Sivan[1]

[1] Department of Geological and Environmental Sciences,
Ben-Gurion University of the Negev,
P. O. Box 653, Beer-Sheva 84105, Israel

[2] Department of Earth Sciences,
University of Cambridge,
Cambridge CB2 3EQ, UK.

[3] Israel Oceanographic and Limnological Research,
National Institute of Oceanography,
Haifa 31080, Israel.

Phone	+44(0)1223333479
Fax	+44(0)1223333450
E-mail	ga307@cam.ac.uk

ABSTRACT

We present new sulfur and oxygen isotope data in sulfate ($\delta^{34}S_{SO4}$ and $\delta^{18}O_{SO4}$ respectively), from globally distributed marine and estuary pore fluids. We use this data with a model of the biochemical steps involved in bacterial sulfate reduction (BSR) to explore how the slope on a $\delta^{18}O_{SO4}$ vs. $\delta^{34}S_{SO4}$ plot relates to the net sulfate reduction rate (nSRR) across a diverse range of natural environments. Our data demonstrate a correlation between the nSRR and the slope of the relative evolution of oxygen and sulfur isotopes ($\delta^{18}O_{SO4}$ vs. $\delta^{34}S_{SO4}$) in the residual sulfate pool, such that higher nSRR results in a lower slope (sulfur isotopes increase faster relative to oxygen isotopes). We combine these results with previously published literature data to show that this correlation scales over many orders of magnitude of nSRR. Our model of the mechanism of BSR indicates that the critical parameter for the relative evolution of oxygen and sulfur isotopes in sulfate during BSR in natural environments is the rate of intracellular sulfite oxidation. In environments where sulfate reduction is fast, such as estuaries and marginal marine environments, this sulfite reoxidation is minimal, and the $\delta^{18}O_{SO4}$ increases more slowly relative to the $\delta^{34}S_{SO4}$. In contrast, in environments where sulfate reduction is very slow, such as deep sea sediments, our model suggests sulfite reoxidation is far more extensive, with as much as 99% of the sulfate being thus recycled; in these environments the $\delta^{18}O_{SO4}$ increases much more rapidly relative to the $\delta^{34}S_{SO4}$. We speculate that the recycling of sulfite plays a physiological role during BSR, helping maintain microbial activity where the availability of the electron donor (e.g. available organic matter) is low.

1. INTRODUCTION

1.1 General

During the anaerobic oxidation of organic matter, bacteria respire a variety of electron acceptors, reflecting both the relative availability of these electron acceptors in the natural environment, as well as the decrease in the free energy yield associated with their reduction (Froelich et al., 1979). The largest energy yield is associated with aerobic respiration (O_2), then denitrification (NO_3^-), then manganese and iron reduction, followed by sulfate reduction (SO_4^{2-}) and finally fermentation of organic matter into methane through methanogenesis (Froelich et al., 1979; Berner, 1980). Due to the high concentration of sulfate in the ocean (at least two orders of magnitude more abundant than oxygen at the sea surface), dissimilatory bacterial sulfate reduction (BSR) is responsible for the majority of oxidation of organic matter in marine sediments (Kasten and Jørgensen, 2000). In addition, the majority of the methane produced during methanogenesis in marine sediments is oxidized anaerobically by sulfate reduction (e.g. Niewöhner et al., 1998; Reeburgh, 2007). The microbial utilization of sulfur in marine sediments is thus critical to the oxidation of carbon in the subsurface.

At a cellular level, the biochemical steps during BSR have been well studied over the past 50 years (Harrison and Thode, 1958; Kaplan and Rittenberg, 1963; Rees, 1973; Farquhar et al., 2003; Brunner and Bernasconi, 2005; Wortmann, et al, 2007; Eckert et al., 2011; Holler et al., 2011). During BSR, bacteria respire sulfate and produce sulfide as an end product. This process consists of at least four major intracellular steps (e.g. Rees, 1973; Canfield, 2001a and Figure 1): during step 1, the extracellular sulfate enters the cell; in step 2, the sulfate is activated with adenosine

triphosphate (ATP) to form Adenosine 5' Phosphosulfate (APS); in step 3, the APS is reduced to sulfite (SO_3^{2-}); and in step 4 the sulfite is reduced to sulfide. It is generally assumed that all four steps are reversible (e.g. Brunner and Bernasconi, 2005; Eckert et al., 2011). The reduction of sulfite to sulfide (step 4) remains the most enigmatic, and may occur in one step with the enzyme dissimilatory sulfite reductase or through the multi-step trithionite pathway producing several other intermediates (e.g. trithionate ($S_3O_6^{2-}$) and thiosulfate ($S_2O_3^{2-}$) -- Kobayashi et al. 1969; Brunner et al. 2005; Sim et al. 2011a; Bradley et al., 2011); although there is evidence that whatever pathway step 4 occurs through, it is also reversible (Trudinger and Chambers, 1973; Eckert et al., 2011, Holler et al., 2011, Tapgaar et al., 2011).

Given that each of the four steps is reversible, understanding the relative forward and backward fluxes at each step and how these fluxes relate to the overall rate of sulfate reduction, is critical for understanding the link between the BSR and the rate of organic matter oxidation. Changes in environmental conditions (e.g. temperature, carbon substrate, pressure) likely impact the relative forward and backward fluxes at each step within the cell as well as the overall rate of BSR, but the relative role of these factors with respect to one another in the natural environment remains elusive. Within the marine subsurface, measurements of sulfate concentrations in sedimentary pore fluids and subsequent diffusion-consumption modeling of the rate of sulfate depletion with depth can be used for calculating the overall rate of sulfate reduction below the ocean floor (e.g. Berner, 1980; D'Hondt et al., 2004; Wortmann, 2006; Wortmann et al., 2007). These sulfate concentration profiles alone, however, cannot provide details about how the individual biochemical steps at a cellular or community level may vary with depth or under different environmental conditions.

A particularly powerful tool for studying these biochemical steps during BSR (hereafter termed the 'mechanism' of BSR) is sulfur and oxygen isotope ratios measured in the residual sulfate pool while sulfate reduction progresses (Mizutani and Rafter, 1973; Fritz et al., 1989; Aharon and Fu, 2000; Aharon and Fu, 2003; Böttcher et al., 1998; Brunner et al., 2005; Turchyn et al., 2006; Wortmann et al., 2007; Farquhar et al., 2008; Turchyn et al., 2010; Aller et al., 2010). With respect to isotopes, we refer to the ratio of the heavier isotope of sulfur or oxygen (^{34}S or ^{18}O) to the lighter isotope (^{32}S or ^{16}O), reported in delta notation relative to a standard (VCDT for sulfur and VSMOW for oxygen) in parts per thousand or permil (‰).

Although both sulfur and oxygen isotopes are partitioned during each intracellular step, their relative behavior (e.g. $\delta^{18}O_{SO4}$ vs. $\delta^{34}S_{SO4}$) in the natural environment is not fully understood. The sulfur isotope composition of sulfate ($\delta^{34}S_{SO4}$) typically increases monotonically as BSR progresses (e.g. Harrison and Thode, 1958; Kaplan and Rittenberg, 1963; Rees, 1973). This occurs because most of the enzymatic steps during BSR preferentially select the lighter sulfur isotope (^{32}S), slowly distilling it into the produced sulfide pool and leaving ^{34}S behind. The magnitude of the sulfur isotope partitioning (fractionation) during the overall process of BSR can be as high as 72‰ (Wortmann et al., 2001; Brunner and Bernasconi 2005; Canfield et al., 2010; Sim et al., 2011a). Theoretical and experimental studies have suggested that this magnitude is a function of microbial metabolism and carbon source (e.g. Brüchert, 2004; Sim et al., 2011b), amount of sulfate available (e.g. Canfield, 2001b; Habicht et al., 2002), and temperature (e.g. Brüchert et al., 2001; Canfield et al., 2006). In addition, previous studies also noted a relationship between the magnitude of the sulfur isotope fractionation and the sulfate reduction rate (Kaplan and Rittenberg, 1964; Rees, 1973; Chambers et al., 1975). This relationship

has been shown in pure culture experiments (e.g. Canfield et al., 2006), batch culture experiments using natural populations (e.g. Stam et al., 2011) and calculated *in situ* using pore fluids profiles (e.g. Aharon and Fu, 2000; Wortmann et al., 2001); in all these studies, higher sulfur isotope fractionation corresponded to slower sulfate reduction rates.

On the other hand, the $\delta^{18}O_{SO4}$ has shown variable behavior during BSR in natural environments. In some cases, the $\delta^{18}O_{SO4}$ exhibits a linear relationship with $\delta^{34}S_{SO4}$, also suggesting a distillation of the light isotope from the reactant sulfate. The magnitude of the oxygen isotope fractionation during this distillation was suggested to be 25% of the magnitude for sulfur isotopes (Rafter and Mizutani 1967), although it has been observed to range between 22% (Mandernack et al., 2003) to 71% (Aharon and Fu, 2000). In most measurements of $\delta^{18}O_{SO4}$ during BSR in the natural environment, however, the $\delta^{18}O_{SO4}$ increases initially until it reaches a constant value and does not increase further, while the $\delta^{34}S_{SO4}$ may continue to increase (e.g. Fritz et al, 1989; Böttcher et al., 1998, 1999; Turchyn et al, 2006; Wortmann, et al, 2007; Aller et al, 2010; Zeebe, 2010). This 'oxygen isotope equilibrium' value (usually between 22 and 30‰ in most natural environments) has been shown to depend on the $\delta^{18}O$ of the ambient water (Fritz et al, 1989; Mizutani and Rafter 1973; Brunner et al., 2005; Mangalo et al, 2007; Mangalo et al, 2008). Because the timescale for oxygen isotope exchange between sulfate and water is exceptionally slow (e.g. Lloyd, 1968), it has been suggested that, during BSR, oxygen isotopes of sulfur intermediate species such as APS and SO_3^{2-} exchange oxygen atoms with water (Fritz et al, 1989; Mizutani and Rafter, 1973). Recent studies have suggested that it is more likely sulfite when bound in the AMP-sulfite complex facilitates this oxygen isotopic exchange (Kohl and Bao 2006; Wortmann et al., 2007;

Brunner et al., 2012; Kohl et al., 2012). This requires that some percentage of the sulfate that is brought into the cell does not get reduced all the way to sulfide but undergoes oxygen isotope exchange with water, reoxidation to sulfate, and release back to the extracellular sulfate pool (Fritz et al, 1989; Mizutani and Rafter 1973; Brunner et al., 2005; Mangalo et al, 2007; Wortmann, et al, 2007; Mangalo et al, 2008; Farquhar et al., 2008; Turchyn et al, 2010; Brunner et al., 2012).

Interpreting the relative evolution of the $\delta^{18}O_{SO4}$ and the $\delta^{34}S_{SO4}$ in the extracellular sulfate pool during BSR in natural environments, and what this relative evolution tells us about the enzymatic steps during sulfate reduction remains confounding. Figure 2 shows schematically how pore fluid sulfate and sulfur and oxygen isotope profiles often look in nature, where pore fluid sulfate concentrations decrease below the sediment-water interface and the oxygen and sulfur isotope ratios of sulfate increase, but may evolve differently relative to one another. One question is what are the factors controlling BSR in natural environments when the coupled sulfur and oxygen isotopes increase linearly (Trend A), compared to when they are decoupled and oxygen isotopes are seen to plateau (Trend B)? A second problem is that the majority of our understanding of the biochemical steps during BSR comes from pure culture studies; how does this understanding translate, if at all, to the study of BSR in the natural environment?

In this paper we will forward this discussion by presenting a compilation of sulfur and oxygen isotopes in pore fluids, including seven new sites collected over a range of different subsurface marine and near-marine environments, covering a broad range of sulfate reduction rates. This will allow us to investigate how the relative behavior of the sulfur and oxygen isotopes varies in these different environments. We will begin with a discussion of modeling sulfur and oxygen isotope evolution during

145 BSR, most of which is a review of previous seminal work. We will then discuss how
146 these models for the biochemical steps during BSR can be applied to pore fluids in the
147 natural environment. Finally, we will present our results, along with a compilation of
148 previously published data into the context of our model.
149
150 **1.2. Kinetic and equilibrium isotope effects on sulfur and oxygen isotopes during**
151 **dissimilatory bacterial sulfate reduction (BSR)**
152 The overall sulfur and oxygen isotope fractionation during BSR should be the
153 integration of the various forward and backward fluxes at each step with any
154 corresponding isotope fractionation at each step, be it kinetic or equilibrium (Figure 1
155 and Rees, 1973). In this section we will outline the previous modeling efforts and the
156 related equations, upon which our model (Section 2) is based. We begin with sulfur
157 isotopes, which have been more extensively studied than oxygen isotopes. The total
158 sulfur isotope fractionation was first calculated by Rees, (1973):

159
$$\varepsilon^{34}S_{total} = \varepsilon^{34}S_{f\_1} + X_1 \cdot \left(\varepsilon^{34}S_{f\_2} - \varepsilon^{34}S_{b\_1}\right) + \ldots$$
$$X_1 \cdot X_2 \cdot \left(\varepsilon^{34}S_{f\_3} - \varepsilon^{34}S_{b\_2}\right) + X_1 \cdot X_2 \cdot X_3 \cdot \left(\varepsilon^{34}S_{f\_4} - \varepsilon^{34}S_{b\_3}\right) \quad (1)$$

160 where $^{34}S_{total}$ is the total expressed sulfur isotope fractionation, $^{34}S_{i\_j}$ is the sulfur
161 isotope fractionation during the forward (i=f) and backward (i=b) reaction j (where
162 j=1…4) and X_k (where k=1,2,3) is the ratio between the backward and forward fluxes
163 of the respective intracellular steps (Figure 1). The overall expressed sulfur isotope
164 fractionation in the residual sulfate pool, according to this model, is always dependent
165 on the isotope fractionation in the first step (the entrance of sulfate into the cell). The
166 fractionation during the subsequent steps can be expressed in the residual sulfate pool
167 only if there is a backward reaction at each step and a flux of sulfate back out of the
168 cell. The overall expressed sulfur isotope fractionation has been linked to various

169 environmental factors that must result in changes in the relative forward and
170 backward fluxes at each step (Rees, 1973; Farquhar et al., 2003; Brunner and
171 Bernasconi, 2005; Canfield et al., 2006; Farquhar et al. 2007; Johnston et al., 2007).

172 The sulfur isotope fractionation for the forward reaction at steps 1, 3 and 4
173 (figure 1), that is, sulfate incorporation into the cell, the reduction of APS to sulfite,
174 and the reduction of sulfite to sulfide, are understood to be -3, 25 and 25‰
175 respectively (all others steps are assumed to have no sulfur isotope fractionation,
176 Rees, 1973). Therefore, equation 1 can be written as:

177 $$\varepsilon^{34}S_{total} = -3‰ + X_1 \cdot X_2 \cdot 25‰ + X_1 \cdot X_2 \cdot X_3 \cdot 25‰ \quad (2)$$

178 In order to generate an expressed sulfur isotope fractionation larger than -3‰, there
179 must be back reactions during at least the first three steps. It has also been observed
180 that the total expressed sulfur isotope fractionation during BSR decreases with
181 increased sulfate reduction rates (e.g. Aharon and Fu, 2000; Canfield, et al, 2006;
182 Sim, et al., 2011b; Stam et al., 2011). This suggests, as previous research has
183 concluded, that as the sulfate reduction rate increases, backward reactions become less
184 significant relative to forward reactions, and the total sulfur isotope fractionation
185 approaches the fractionation associated with transfer of sulfate through the cell wall
186 (Canfield, 2001).

187 Equation 2 predicts a maximum possible expressed sulfur isotope
188 fractionation during BSR of 47‰. However, particularly in natural environments, the
189 measured sulfur isotope fractionation can often exceed these values, reaching up to
190 72‰ (Habicht and Canfield, 1996; Wortmann et al, 2001). Such large offsets are
191 often attributed to repeated redox cycles of sulfur in the subsurface: the initial
192 reduction of sulfate through BSR, the subsequent reoxidation of sulfide to elemental
193 sulfur, followed by sulfur disproportionation to sulfate and sulfide, which produces

194 more sulfate for BSR (Canfield and Thamdrup, 1994). These repeated cycles allow
195 for a larger overall expressed sulfur isotope fractionation. Another explanation for the
196 large sulfur isotope fractionations observed in nature is the trithionite pathway, in
197 which the reduction of sulfite to sulfide (step 4) proceeds through multiple steps rather
198 than one (Kobayashi et al. 1969; Brunner and Bernasconi 2005; Johnston et al., 2007;
199 Sim et al. 2011a; Bradley et al., 2011). This could induce additional sulfur isotope
200 fractionation and result in expressed sulfur isotope fractionation as large as 72‰
201 (Brunner and Bernasconi, 2005; Sim et al., 2011a).

202 Defining a relationship like Equation 1 for oxygen isotopes is somewhat more
203 difficult because both kinetic oxygen isotope fractionation and equilibrium oxygen
204 isotope fractionation need to be considered. If we first consider the case where kinetic
205 oxygen isotope fractionation is the only process affecting $\delta^{18}O_{SO4}$ during BSR, then
206 the overall oxygen isotope fractionation can be formulated similar to Equation 1
207 (Brunner et al., 2005):

208
$$\varepsilon^{18}O_{total} = \varepsilon^{18}O_{f\_1} + X_1 \cdot \left(\varepsilon^{18}O_{f\_2} - \varepsilon^{18}O_{b\_1}\right) + \ldots$$
$$X_1 \cdot X_2 \cdot \left(\varepsilon^{18}O_{f\_3} - \varepsilon^{18}O_{b\_2}\right) + X_1 \cdot X_2 \cdot X_3 \cdot \left(\varepsilon^{18}O_{f\_4} - \varepsilon^{18}O_{b\_3}\right) \quad (3)$$

209 In this case, the $\delta^{18}O_{SO4}$ and $\delta^{34}S_{SO4}$ in the residual sulfate pool will evolve in a
210 similar manner and a linear relationship should emerge when plotting one isotope
211 versus the other ('Trend A' in figure 2). The ratio between $^{18}O_{total}$ and $^{34}S_{total}$ would
212 then be equal to the slope of this line.

213 However, the $\delta^{18}O_{SO4}$ also exhibits equilibrium oxygen isotope fractionation
214 during BSR, often linked to the isotopic composition of the ambient water (Mizutani
215 and Rafter, 1973; Fritz et al., 1989; Brunner et al., 2005; Mangalo et al., 2007,2008;
216 Farquhar et al., 2008; Turchyn et al., 2010; Zeebe, 2010; Brunner et al., 2012). Field
217 studies have found that this 'equilibrium isotope exchange' results in the $\delta^{18}O_{SO4}$ in

the residual sulfate pool evolving to a value between 22 and 30‰, across a range of natural environments (Böttcher et al., 1998, 1999; Turchyn et al., 2006; Wortmann et al., 2007; Aller et al., 2010). The fact that the $\delta^{18}O_{SO4}$ reaches a constant value is interpreted as oxygen isotope exchange between intracellular sulfur intermediates and water. The measured oxygen isotope equilibrium value therefore includes the kinetic oxygen isotope fractionation associated with each step, the equilibrium partitioning of oxygen isotopes between intracellular water and the intermediate sulfur species, and any oxygen isotope fractionation associated with the assimilation of oxygen atoms from water during reoxidation. Because of the myriad of factors impacting the observed equilibrium value of $\delta^{18}O_{SO4,}$ the measured value in the residual sulfate $\delta^{18}O_{SO4}$ is termed the 'apparent equilibrium' (Wortmann, et al, 2007). Turchyn et al. (2010) formulated a mathematical term for the apparent equilibrium of $\delta^{18}O_{SO4,}$ assuming full isotope equilibrium between intra-cellular intermediates and water, and kinetic oxygen isotope fractionation only during the reduction of APS to sulfite (step 3):

$$\delta^{18}O_{SO4(A.E)} = \delta^{18}O_{H2O} + \varepsilon^{18}O_{exchange} + \frac{1}{X_3} \cdot \varepsilon^{18}O_{f\_3} \quad (4)$$

where $\delta^{18}O_{SO4(A.E)}$ is the isotopic composition of sulfate at 'apparent equilibrium', $\delta^{18}O_{(H2O)}$ is the isotopic composition of the ambient water, $^{18}O_{exchange}$ is the oxygen isotope fractionation between sulfite in the AMP-sulfite complex and ambient water, X_3 is the ratio between the backward and forward fluxes at Step 3 as in Equation 1 (Figure 1) and $^{18}O_{f\_3}$ is the kinetic oxygen isotope fractionation associated with APS reduction to sulfite.

In summary, current models for BSR suggest that sulfur and oxygen isotopes in the residual sulfate pool respond to changes in the relative forward and backward

242 rates of reaction, and isotope fractionation associated with each step during BSR. The
243 relative contribution of these various forward and backward fluxes and their
244 individual isotope fractionation should be expressed by different relationships
245 between $\delta^{18}O_{SO4}$ and $\delta^{34}S_{SO4}$ in sulfate as BSR progresses. When the kinetic oxygen
246 isotope fractionation outcompetes the equilibrium oxygen isotope fractionation, the
247 plot of $\delta^{18}O_{SO4}$ vs. $\delta^{34}S_{SO4}$ should exhibit a linear relationship ('trend A' in Figure 2b --
248 e.g. Mizutani and Rafter, 1969; Aharon and Fu, 2000; Aharon and Fu, 2003;
249 Mandernack et al, 2003). When the equilibrium isotope effect dominates, a plot of
250 $\delta^{18}O_{SO4}$ vs. $\delta^{34}S_{SO4}$ will tend concavely towards the 'apparent equilibrium' ('trend B'
251 in Figure 2b -- e.g. Böttcher et al., 1998, 1999; Turchyn et al., 2006; Aller et al.,
252 2010). In between these two extremes, the relative intensity of the kinetic and
253 equilibrium isotopic effects will determine the moderation of the curve and how
254 quickly it reaches equilibrium, if at all.

255 It has been suggested that this relative evolution of the $\delta^{18}O_{SO4}$ vs. $\delta^{34}S_{SO4}$ during
256 BSR should be connected to the overall sulfate reduction rate (Böttcher et al., 1998,
257 1999; Aharon and Fu, 2000, Brunner et al., 2005) where the steeper the slope on a
258 plot of $\delta^{18}O_{SO4}$ vs. $\delta^{34}S_{SO4}$, the slower the sulfate reduction rate. This suggestion was
259 elaborated upon by Brunner et al. (2005), who formulated a model for mass flow
260 during BSR. In this work, Brunner et al. (2005) deduced that the overall SRR is
261 important for the relative evolution of $\delta^{18}O_{SO4}$ and $\delta^{34}S_{SO4}$, but that the rate of oxygen
262 isotope exchange between sulfur intermediates and water, and the relative forward
263 and backward fluxes at each step further modifies the evolution of $\delta^{18}O_{SO4}$ vs. $\delta^{34}S_{SO4}$.

264 The above models as developed previously have applied largely to understanding
265 the relative forward and backwards steps during BSR in pure culture. We hypothesize
266 that we can investigate a wider range of sulfate reduction rates in the natural

267 environment, and thus are poised to be able to address this relationship more
268 completely. This is a particularly good juncture to investigate this further as the
269 models for BSR and the relationship between the mechanism and the couple sulfate
270 isotopes have experienced several significant advances in recent years (e.g. Brunner et
271 al., 2005; 2012; Wortmann et al., 2007). Although there are potentially other
272 processes in natural environments that may impact the measured $\delta^{18}O_{SO4}$ vs. $\delta^{34}S_{SO4}$ –
273 for example anaerobic pyrite oxidation (e.g. Balci et al., 2007; Brunner, et al., 2008;
274 Heidel and Tichomirowa, 2011; Kohl and Bao, 2011), or sulfur disproportionation
275 (Cypionka et al., 1998; (Böttcher et al, 2001; Böttcher and Thamdrup, 2001; Aharon
276 and Fu, 2003; Böttcher et al, 2005; Blake et al, 2006; Aller et al, 2010), we feel there
277 is significant knowledge to be gained by revisiting the mechanism of BSR as deduced
278 from geochemical analysis of pore fluids.

279 The use of the evolution of the $\delta^{18}O_{SO4}$ vs. $\delta^{34}S_{SO4}$ to inform the biochemical steps
280 during BSR has been applied in two previous studies. Wortmann et al, (2007)
281 produced a detailed study of an ODP site off the coast of southern Australia and
282 Turchyn et al, (2006) studied eleven ODP sites off the coasts of Peru, Western Africa
283 and New Zealand. Both studies found a rapid increase in the $\delta^{34}S_{SO4}$, while the
284 $\delta^{18}O_{SO4}$ increased and then leveled off (similar to 'trend B' in Figure 2). Both
285 Wortmann et al. (2007) and Turchyn et al. (2006) used their data with reactive
286 transport models to calculate the relative forward and backward fluxes through
287 bacterial cells during BSR. These studies, which greatly advanced our understanding
288 of *in situ* BSR, focused on deep-sea sediments, with necessarily slow sulfate reduction
289 rates. Furthermore, both of these studies considered only one branching point within
290 the microbial cell, whereas more recent models of the mechanism of BSR have

invoked the importance of at least two branching points to help explain the decoupled sulfur and oxygen isotopes during BSR (Brunner et al., 2005; 2012).

In this paper, we will present sulfur and oxygen isotopes of pore fluid sulfate from 7 new sites with sulfate reduction rates that span many orders of magnitude. We will combine our new data with previously published results of subsurface environments where sulfur and oxygen isotopes in sulfate have been reported. We will use a model derived from the equations above, to understand how the relative evolution of sulfur versus oxygen isotopes in pore fluid sulfate inform us about the intracellular pathways and rates involved in BSR.

2 MODEL FOR OXYGEN ISOTOPE DURING BSR

2.1 The proposed model for oxygen isotopes in sulfate

Our model for oxygen isotopes in sulfate is derived from the work of Brunner et al. (2005, 2012). In order to understand the relative evolution of sulfur and oxygen isotopes in sulfate during BSR in pure culture, Brunner et al. (2005, 2012) solved a time dependent equation in which the oxygen isotope exchange between sulfur intermediates and ambient water and the cell specific sulfate reduction rates are the ultimate factors controlling the slope of $\delta^{18}O_{SO4}$ vs. $\delta^{34}S_{SO4}$ during the onset of BSR. For the purpose of this study (as applied to natural environments rather than pure cultures) we reconsider this model in three ways. First, the cell specific sulfate reduction rate varies over orders of magnitudes in different natural environments, yet the relative evolution of $\delta^{18}O_{SO4}$ vs. $\delta^{34}S_{SO4}$ plot versus depth may exhibit the same pattern. Therefore, we suggest that any time dependent process related to the isotope

312 evolution (e.g. the rate of the oxygen isotopic exchange between ambient water and
313 sulfur intermediate such as sulfite) is faster than the other biochemical steps during
314 BSR. Second, in the models of Brunner et al. (2005, 2012) the equilibrium value for
315 the $\delta^{18}O_{SO4}$ depended critically on the value of $\delta^{18}O$ of the ambient water. However,
316 the equilibrium value for $\delta^{18}O_{SO4}$ in natural environments shows a range (22-30‰)
317 that cannot be explained only by the variation in $\delta^{18}O$ of the ambient water (which
318 ranges from 0 to -4‰). It was initially suggested that these equilibrium values may
319 reflect oxygen isotope equilibrium at different temperatures (Fritz et al., 1989)
320 although more recent studies have shown that the temperature effect is small (~2‰
321 between 23 to 4 C -- Brunner et al., 2006; Zeebe, 2010). Temperature may impact the
322 relative intracellular fluxes during BSR (Canfield et al., 2006), and this will change
323 the apparent equilibrium value (Turchyn et al., 2010). For our model, therefore, we
324 attribute the change in the $\delta^{18}O_{SO4}$ to change in the mechanism of the BSR and not to
325 changes in the $\delta^{18}O$ of the water. Third, the model of Brunner el al. (2005, 2012)
326 ruled out a linear relationship between $\delta^{18}O_{SO4}$ and $\delta^{34}S_{SO4}$ which has not been
327 observed in pure culture. Our model will need to account for a linear relationship,
328 which has been observed in natural environments.

329 To address these issues, we remove the characteristic timescale used by
330 Brunner et al. (2005, 2012) for the cell-specific sulfate reduction rate and focus
331 instead on how the different fluxes at each step impact the evolution of $\delta^{18}O_{SO4}$ vs.
332 $\delta^{34}S_{SO4}$. We further allow changes in the equilibrium values of the $\delta^{18}O_{SO4}$ due to a
333 combination of equilibrium and kinetic oxygen isotope effects (apparent equilibrium)
334 rather than through a change in the $\delta^{18}O$ of the ambient water.

335 The assumptions in our model include:

The system is in steady state. This means SRR = $f_i - b_i$ (where i=1,2,3—figure 1).

We model oxygen isotopic exchange between ambient water and the sulfite (Betts and Voss, 1970; Horner and Connick, 2003), recognizing that this exchange may occur when sulfite is already bound in the AMP-sulfite complex. This oxygen isotope exchange contributes 3 oxygen atoms to the sulfate that will ultimately be produced during reoxidation, while the fourth oxygen atom is gained during the reoxidation of the AMP-sulfite complex to sulfate (Wortmann et al., 2007; Brunner et al., 2012).

Oxygen isotopic exchange was considered to be much faster with respect to other biochemical steps, which means, that for any practical purpose, the sulfite is constantly in isotopic equilibrium with the ambient water. This results in a solution that is independent of the timescale of the problem. This s because the timescale for this isotope exchange, given intracellular pH (6.5-7 — Booth, 1985), should shorter than minutes (Betts and Voss, 1970).

The kinetic oxygen isotopic fractionation during the reduction of APS to sulfite (f_3) is equal to 25% of the sulfur isotope fractionation ($^{18}O_{f\_3}$: $^{34}S_{f\_3}$=1:4) (Mizutani and Rafter, 1969)**.** This value for the kinetic oxygen isotope fractionation is the lowest value that was found in lab experiments, and therefore we consider it to be the closest to the real ratio between $^{18}O_{f\_3}$ and $^{34}S_{f\_3}$. This is assumption has not been made by Brunner et al. (2005, 2012) and allows our model to simulate a linear relationship between $\delta^{18}O_{SO4}$ and $\delta^{34}S_{SO4}$.

359 Any kinetic oxygen isotope fractionation in step 4 (the reduction of sulfite to
360 sulfide) is not significant for oxygen isotopes, since oxygen isotope exchange
361 during the back reaction (step 3) resets the $\delta^{18}O$ of the sulfite.
362 We simplified step 4 by making it unidirectional. We are able to do this
363 because recent work has suggested that even if sulfide concentrations are high
364 (>20 mM), only ~10% of the sulfide is re-oxidized (Eckert et al., 2011) which
365 is insignificant with respect to the overall recycling of other sulfur
366 intermediates (Wortmann et al., 2007; Turchyn et al., 2006).
367
368 The full derivation of the model equations using these assumptions, and similar to the
369 derivation in Brunner et al., 2012, is in Appendix A and yields the following
370 continuous solution for $^{18}O_{SO4(t)}$ as function of $^{34}S_{SO4(t)}$:

371
$$\delta^{18}O_{SO4(t)} = \begin{cases} \frac{\varepsilon^{18}O_{total}}{\varepsilon^{34}S_{total}} \cdot \left(\delta^{34}S_{SO4(t)} - \delta^{34}S_{SO4(0)}\right) + \delta^{18}O_{SO4(0)} & X_1 \cdot X_2 \cdot X_3 = 0 \\ \delta^{18}O_{SO4(A.E)} - \exp\left(-\theta_O \cdot \frac{\delta^{34}S_{SO4(t)} - \delta^{34}S_{SO4(0)}}{\varepsilon^{34}S_{total}}\right) \cdot \left(\delta^{18}O_{SO4(A.E)} - \delta^{18}O_{SO4(0)}\right) & 0 < X_1 \cdot X_2 \cdot X_3 < 1 \end{cases} \quad (5)$$

372 where $^{18}O_{SO4(t)}$ is the oxygen isotopic composition of the residual sulfate at time t,
373 $^{18}O_{SO4(A.E)}$ is the oxygen isotopic composition of the residual sulfate at apparent
374 equilibrium (see section 1.2 above) and $^{18}O_{SO4(0)}$ is the oxygen isotope composition of
375 the initial sulfate. The $^{34}S_{SO4(t)}$ is the sulfur isotopic composition of the residual
376 sulfate at time t, $^{34}S_{SO4(0)}$ is the initial sulfur isotopic composition of the residual
377 sulfate, $^{34}S_{total}$ $^{18}O_{total}$ are the overall expressed sulfur and oxygen isotope fractionation,
378 respectively, and $_O$ is a parameter initially formulated by Brunner et al. (2005, 2012).
379 This parameter ($_O$) measures the ratio between the apparent oxygen isotope exchange
380 and sulfate reduction rate. However, since we assumed constantly full oxygen

isotopic equilibrium between sulfite and ambient water, in our case this parameter should only be a function of the ratio between the backward and forward fluxes, and is less impacted by changes in the initial isotopic composition of the sulfate, the isotopic composition of the water, the kinetic isotope fractionation factor for step 3, or the magnitude of the fractionation factor during oxygen isotopic exchange (See appendix A).

The solution to our model (Equation 5) suggests two distinct phases for the relative evolution of $\delta^{18}O_{SO4}$ vs. $\delta^{34}S_{SO4}$ during BSR:

1. Apparent linear phase. This phase refers to the initial stage of BSR, where the sulfur and oxygen isotopic compositions increase in the residual sulfate pool at a constant ratio (see also 'trend b' in figure 2b). The first-order Taylor series expansion around the point $(\delta^{34}S_{SO4}, \delta^{18}O_{SO4}) = (\delta^{34}S_{SO4(0)}, \delta^{18}O_{SO4(0)})$ of Equation 5 provides information about the behavior of $\delta^{18}O_{SO4}$ vs. $\delta^{34}S_{SO4}$ at the onset of the BSR and is equal to:

$$\delta^{18}O_{SO4(t)} = \delta^{18}O_{SO4(0)} + \left(\delta^{18}O_{SO4(A.E)} - \delta^{18}O_{SO4(0)}\right) \cdot \theta_O \cdot \frac{\delta^{34}S_{SO4(t)} - \delta^{34}S_{SO4(0)}}{\varepsilon^{34}S_{total}} \quad (6)$$

We term this the slope of the apparent linear phase (SALP) in $\delta^{18}O_{SO4}$ vs. $\delta^{34}S_{SO4}$ space:

$$SALP = \theta_O \cdot \frac{\delta^{18}O_{SO4(A.E)} - \delta^{18}O_{SO4(0)}}{\varepsilon^{34}S_{total}} \quad (7)$$

This equation suggests that the SALP is directly proportional to θ_O. SALP is also inversely proportional to $^{34}S_{total}$.

2. Apparent equilibrium phase. This phase refers to the later phase of BSR where the oxygen isotope composition of the residual sulfate pool reaches a constant value, while the sulfur isotope composition continues to increase (Wortmann, et al., 2007 and Turchyn et al., 2010, see also 'trend b' in figure 2b). Here we modified the term for the apparent equilibrium of $\delta^{18}O_{SO4}$ that was given by Turchyn et al. (2010), and also presented in Equation 4. This is because the term that was formulated by Turchyn et al. (2010) assumed that the uptake of sulfate into the cell (step 1) involves no kinetic isotope effect for oxygen, although a kinetic isotope effect for sulfur does exist. If there is a kinetic oxygen isotope fractionation during sulfate uptake, (step 1) and during the reduction of APS to sulfite (step 3), then the apparent equilibrium value of $\delta^{18}O_{SO4}$ ($\delta^{18}O_{SO4(A.E)}$) is given by (See Appendix B for the full derivation):

$$\delta^{18}O_{SO4(A.E)} = \delta^{18}O_{H2O} + \varepsilon^{18}O_{exchange} + \frac{\varepsilon^{18}O_{f\_1}}{X_1 \cdot X_3} + \frac{\varepsilon^{18}O_{f\_3}}{X_3} \quad (8)$$

Previous studies have used plots of θ_O vs. $^{34}S_{total}$ to investigate the mechanism of BSR (Turchyn et al., 2010; Brunner et al., 2012). There is an ambiguity with calculating X_1 and X_2 separately using isotopes since there is understood to be no isotopic fractionation at step 2 (e.g. Rees et al., 1972). Therefore, if we consider the two main intracellular branching points in the schematic in figure 1 (similar to Farquhar et al., 2003; Canfield et al., 2006), we can rethink the reaction schematic in figure 1 without the APS intermediate as shown in figure 3 (another way to work around this ambiguity is by merging step 1 and 2 into one single step. This choice would also have no impact on the calculation). In this case, θ_O is equal to (after Brunner et al., 2012):

$$\theta_O = \frac{X_1 \cdot X_3}{1 - X_1 \cdot X_3} \quad (9)$$

and the $^{34}S_{total}$ according to Rees, (1973) is:

$$\varepsilon^{34}S_{total} = -3 + 25 \cdot X_1 + 25 \cdot X_1 \cdot X_3 \quad (10)$$

We acknowledge the fact that recent studies have found sulfur fractionation much higher than 47‰ (e.g. Habicht and Canfield, 1996; Wortmann et al, 2001; Sim et al., 2011a), which is the maximum fractionation that equation 10 predicts. This however, can be solved by adding another branching point and not by simply adding the additional fractionation (about 50‰) to step 3 (Brunner et al., 2012). Since it is not clear what are the exact environmental constraints activate the trithionite pathway, at this point, we stick to the traditional pathway and will examine if it can simulate pore fluid $\delta^{18}O_{SO4}$ and $\delta^{34}S_{SO4}$.

These equations provide unique solutions for X_1 (the ratio between sulfate being brought in and out of the cell) and X_3 (the ratio between the forward and backward fluxes at step 3). Because θ_O and $^{34}S_{total}$ can be written in terms of X_1 (the ratio between sulfate being brought in and out of the cell) and X_3 (the ratio between the forward and backward fluxes at step 3), we can calculate $^{34}S_{total}$ and θ_O for a range of X_1 and X_3 values and contour them on a θ_O vs. $^{34}S_{total}$ diagram (Figure 4). This allows us to depict variations in θ_O vs. $^{34}S_{total}$ in terms of variations in X_1 and X_3 during BSR. X_1 provides nearly vertical contours in θ_O vs. $^{34}S_{total}$ space, suggesting that variations in the flux at step 1 are the main cause for changes in the expressed sulfur isotope fractionation ($^{34}S_{total}$), especially at lower values of X_3. On the other hand, X_3 contours horizontally, suggesting that changes in this step cause the most significant impact on θ_O. The plot of θ_O vs. $^{34}S_{total}$ (Figure 4) has similarities with the

theoretical $\lambda_{H2S\text{-}SO4}$ vs. $1000 \cdot \ln(r^{34}_{H2S} \backslash r^{34}_{SO4})$ diagram designed by Farquhar et al. (2003). Both diagrams are based on multiple reaction pathways for sulfate within the bacterial cell. The rate and direction of these reactions control the sulfur and oxygen isotope evolution of sulfate. We can use the θ_O vs. $^{34}S_{total}$ to interpret the mechanism of BSR for our data and previously published work. An extension would be to investigate the mechanism using a $\lambda_{H2S\text{-}SO4}$ vs. $1000 \cdot \ln(r^{34}_{H2S} \backslash r^{34}_{SO4})$ diagram as more r^{33}_{SO4} data becomes available.

2.2 Testing the proposed model

Our changes to the existing models of bacterial sulfate reduction now allow it to be applied to a wider range of timescales and parameter space observed in natural environments. We will apply it now to a pure culture study to show its applicability. Mangalo et al. (2008) carried out five pure culture experiments, with *Desulfovibrio desulfuricans* and ^{18}O enriched water (about 700‰) and varied the nitrite concentration. Nitrite is an inhibitor for the enzyme dissimilatory sulfite reductase used in Step 4 (Greene et al., 2003). Increased nitrite concentrations should, therefore, lead to less reduction of sulfite to sulfide and potentially more recycling of sulfite back to sulfate (Figure 1). In other words, the higher the nitrite concentration, the higher the backward flux at step 3 (the reoxidation of sulfite to APS), and θ_O should increase.

The $\delta^{18}O_{H2O}$ in these experiments was strongly enriched in ^{18}O (700‰ Mangalo et al., 2008). This allows us to investigate the contribution of each step during BSR to the evolution of $\delta^{18}O_{SO4}$ vs. $\delta^{34}S_{SO4}$, since it significantly reduces the uncertainty on the expected $\delta^{18}O_{SO4(A.E)}$. We calculated the θ_O for each experiment in Mangalo et al. (2008) using equation 7. The SALP was obtained from a linear regression of $\delta^{18}O_{SO4}$

vs. $\delta^{34}S_{SO4}$ presented in Mangalo et al. (2008) and the sulfur isotope fractionation ($^{34}S_{total}$) was taken from their calculation. The Mangalo et al. (2008) data is presented on the θ_O vs. $^{34}S_{total}$ diagram (Figure 4).

By changing the nitrite concentration, Mangalo et al. (2008) were indeed able to affect the value of X_3, the ratio of the forward and backward fluxes at step 3. Our analysis shows that the SALP of each experiment shows a strong correlation to the nitrite concentration (Figure 5a) and with X_3 (Figure 5b) (R^2=0.9987). However, it seems that there is a poor correlation between X_1 and the SALP (Figure 5b) (R^2=0.3002). This suggests that X_3 is directly responding to nitrite concentration, confirming that nitrite was inhibiting sulfite reduction at step 4 (f_4 decreases) and resulting in more sulfite being reoxidized to APS (b_3 increases). In addition, these results suggest that X_3 is the dominant factor controlling the SALP in these experiments.

Analysis of the Mangalo et al. (2008) data shows that the model may help calculate X_1 and X_3 during BSR in pure culture. Application to the natural environment still requires consideration of how the expression of the mechanism of BSR will be seen within pore fluid profiles, which we will consider in Section 5. First we will present our analytical methods and results.

3. METHODS

3.1 Study Sites

We present pore fluid profiles from seven new sites (see Map, Figure 6). The first two sites, Y1 and Y2 are in the Yarqon Stream estuary, Israel (Figure 6b), with a

water depth of ~2 m. Cores were taken using a gravity corer, total core lengths were 29 and 9cm, for Y1 and Y2 respectively. The Yarqon estuary sediments have a very high organic carbon content of 2.5% and are in contact with brackish bottom waters (~19 g Cl l^{-1}), due to seawater penetration into the estuary.

Cores were collected at three sites on the shallow shelf of the Eastern Mediterranean Sea off the Israeli coast; Sites HU, 130 and BA1 (Figure 6b), with water depths of 66 m, 58 m and 693 m respectively. Total core lengths for the three sites were 234, 254 and 30 cm respectively. The sediment from site BA1 was collected using a box corer, while a piston corer was used for sites 130 and HU. The organic carbon content at these sites ranges from ~0.5-1.0%. Finally, pore fluid profiles are also presented from advanced piston cores collected by the Ocean Drilling Program (ODP) at ODP Sites 1052 and 807. Site 1052 (Leg 171B), is located on Blake Nose (NW Atlantic Ocean) at a water depth of 1345m, with a total sediment penetration of 684.8 m (60.2% recovery). Site 807 (Leg 130) (Figure 6a), is located on the Ontong-Java Plateau (tropical NW Pacific) at a water depth of 2805 m with a total sediment penetration of 822.9 m (87.1% recovery). The organic carbon content at Site 1052 it is below 1%, while at Site 807 ranges between 0.02-0.6%.

3.2 Analytical Methods

The samples from the Yarqon estuary and the Eastern Mediterranean sites were processed at Ben Gurion University of the Negev, Israel, usually on the same day as coring. The cores were split into 1 cm slices under an argon purge. The pore fluids were extracted from each cm slice by centrifuging under an argon atmosphere to avoid oxygen contamination. The samples were acidified and purged with argon to remove sulfides and prevent their oxidation to sulfate. The sulfate concentration in

521 the pore fluids from the Yarqon estuary was measured by high performance liquid
522 chromatography (HPLC, Dionex DX500) with a precision of 3%. The total sulfur
523 (assumed to be only sulfate) concentrations from the Eastern Mediterranean were
524 measured by inductivity coupled plasma-atomic emission (ICP-AES, P-E optima
525 3300) with a precision of 2%.

526 The ODP sediments were handled using standard shipboard procedures.
527 Sulfate concentrations of the pore fluids from the ODP Sites were measured by
528 Dionex ion chromatograph onboard the ship. Pore fluid sulfate from the Yarqon
529 estuary, the Eastern Mediterranean and the ODP sites were then precipitated as
530 barium sulfate (barite) by adding a saturated barium chloride solution. The barite was
531 subsequently rinsed with acid and deionized water and set to dry in a 50 C oven.

532 The sulfur and oxygen isotope composition of the pore fluid sulfate were
533 analyzed in the Godwin Laboratory at the University of Cambridge. The barite
534 precipitate was pyrolyzed at 1450°C in a Temperature Conversion Element Analyzer
535 (TC/EA), and the resulting carbon monoxide (CO) was measured by continuous flow
536 GS-IRMS (Delta V Plus) for its $\delta^{18}O_{SO4}$. For the $\delta^{34}S_{SO4}$ analysis the barite was
537 combusted at 1030°C in a Flash Element Analyzer (EA), and resulting sulfur dioxide
538 (SO_2) was measured by continuous flow GS-IRMS (Thermo, Delta V Plus). Samples
539 for $\delta^{18}O_{SO4}$ were run in replicate and the standard deviation of these replicate analyses
540 was used (< 0.4‰). The error for $\delta^{34}S_{SO4}$ was determined using the standard deviation
541 of the standard NBS 127 at the beginning and the end of each run (~ 0.2‰). Samples
542 for both $\delta^{18}O_{SO4}$ and $\delta^{34}S_{SO4}$ were corrected to NBS 127 (8.6‰ for $\delta^{18}O_{SO4}$ and
543 20.3‰ for $\delta^{34}S_{SO4}$). A second laboratory derived barite standard was run for $\delta^{18}O_{SO4}$
544 (16‰) to correct for linear changes during continuous flow over a range of $\delta^{18}O_{SO4}$
545 values and to map our measurements more accurately in isotope space. Since the bulk

546 of our $\delta^{18}O_{SO4}$ data falls between 8 and 21‰, these standards were appropriate for the
547 isotope range of interest.

4. FIELD RESULTS

548 The pore fluid sulfate concentrations and oxygen and sulfur isotope compositions
549 for the seven new sites are shown in Figure 7. The cores from the Yarqon estuary
550 (Y1, 29 cm and Y2, 9 cm, figure 7a-7c) are similar and show almost total depletion in
551 pore fluid sulfate (site Y1, figure 7c). As sulfate concentrations decrease, both the
552 $\delta^{18}O_{SO4}$ and $\delta^{34}S_{SO4}$ of the sulfate increase. At the greater depths, $\delta^{34}S_{SO4}$ continues to
553 increase, while $\delta^{18}O_{SO4}$ reaches a constant value of 23-24‰ (site Y1 Figure 7c).
554 The results from sites BA1 (30 cm) HU (234 cm) and P130 (254 cm) are
555 shown in Figure 7e-7f. There is a maximum of 40% consumption of sulfate, within
556 the upper 234 cm at Site HU, and within 250 cm at Site P130. Both the $\delta^{18}O_{SO4}$ and
557 $\delta^{34}S_{SO4}$ increase with depth at both sites: the $\delta^{34}S_{SO4}$ increases to 30.3‰ and the
558 $\delta^{18}O_{SO4}$ increases to 19.0‰ at site HU, while at site P130 the $\delta^{34}S_{SO4}$ increases to
559 38.8‰ and the $\delta^{18}O_{SO4}$ increases to 24.0‰. At site BA1, $\delta^{18}O_{SO4}$ and $\delta^{34}S_{SO4}$ both
560 increase while the pore fluid sulfate concentration decreases (Figure 7d-7f)
561 In ODP Sites 807 and 1052, pore fluid sulfate concentrations remain constant
562 in the upper 30 m, and then decrease over the next ~200 m by 25 and 50%
563 respectively (Figure 7g-7i). At both Sites, the $\delta^{34}S_{SO4}$ increases with decreasing
564 sulfate concentrations, to values of 28-29‰ at ~300 m. The $\delta^{18}O_{SO4}$ also increases to
565 22-23‰ at both Sites.

5. DISCUSSION

5.1 Applying our time-dependent closed system model to pore fluid profiles

In this section we discuss the use of our model of BSR (Section 2.1 and 2.2) to understand what controls the relative evolution of $\delta^{18}O_{SO4}$ vs. $\delta^{34}S_{SO4}$ in the natural environment. Applying what is effectively a "closed system" model to an "open system" (environmental pore fluids) requires understanding the physical parameters that control each of the sulfate species concentrations (in our case $^{34}S^{16}O_4^{2-}$, $^{32}S^{18}O^{16}O_3^{2-}$ and $^{32}S^{16}O_4^{2-}$) within the fluids in the sediment column (Jørgensen, 1979; Chernyavsky and Wortmann, 2007; Wortmann and Chernyavsky, 2011).

In this study we utilize SALP, that is the relative change of $\delta^{18}O_{SO4}$ vs. $\delta^{34}S_{SO4}$, rather than the $\delta^{18}O_{SO4}$ value during apparent equilibrium although both hold information about the mechanism of the BSR (see equation 7 and 8). Focusing on SALP enables investigating the mechanism of BSR from sites that were not cored deep enough to observe apparent equilibrium (e.g. Mediterranean Sea sediments from this study, Figure 7d-f). Also, it is not clear whether the $\delta^{18}O_{SO4}$ really reaches equilibrium values at some sites (e.g. the ODP Sites, Figure 7g-i).

The outstanding question is how can we apply SALP as observed in the relative evolution of the $\delta^{18}O_{SO4}$ and $\delta^{34}S_{SO4}$ in the pore fluids to the model for the biochemical steps during BSR as derived for pure cultures? How do you bridge the gap between the "closed system" equations and the application to the "open system"? To explore this, we will briefly explore how SALP changes between closed and open systems in two extreme cases: (a) Deep-sea temperature (2 C), low sedimentation rate (10^{-3} cm·year^{-1}) and slow net sulfate reduction rate (low as 10^{-12} mol·cm^{-3}·year^{-1}), typical of deep-sea environments versus (b) Surface temperature (25 C), high

589 sedimentation rate (10^{-1} cm·year^{-1}) and high net sulfate reduction rate (5 10^{-4} mol·cm^{-3}·year^{-1}) conditions similar to shallow marginal-marine environments. In each case we have calculated the "closed system" solution for a given mechanism, or intracellular fluxes during BSR, and then separately calculated the "open system" for the same mechanism give the natural conditions described above. For the entire model description see Appendix C.

595 Figure 9 presents the calculated open system versus closed system SALP for the two extreme environments, as function of the change in X_3 (where X_1 is fixed and equal to 0.99). It can be seen that in applying the close system solution to the open system can lead to underestimation of as much as 10% in the value of X_3 (For changes in X_1, the misestimate will be similar in magnitude). Although there are vastly different physical parameters between these two synthetic sites, the resulting calculated SALPs are not significantly different. This similarity in calculated SALP is because the main difference moving to an open system from a closed system is the change the relative diffusion flux of any of the isotopologues. We conclude that we can read the SALP from $\delta^{18}O_{SO4}$ and $\delta^{34}S_{SO4}$ pore fluid profiles (e.g. Figure 2) and apply our closed system model to understand the mechanism, with the caveat that we have error bars on our resulting interpretation.

5.2 What controls the relative evolution of $\delta^{18}O_{SO4}$ vs. $\delta^{34}S_{SO4}$ in marine sediments during BSR

607 It has been suggested that in the natural environment as well as in pore fluids, the relative evolution of $\delta^{18}O_{SO4}$ vs. $\delta^{34}S_{SO4}$ (SALP) is connected to the overall sulfate reduction rate (Böttcher et al., 1998, 1999; Aharon and Fu, 2000; Brunner, et al, 2005). We further suspect that the relative evolution provides information about the

611 mechanism, or individual intracellular steps, during BSR. A plot of our data in
612 $\delta^{18}O_{SO4}$ vs. $\delta^{34}S_{SO4}$ space displays a close-to-linear relationship between $\delta^{18}O_{SO4}$ and
613 $\delta^{34}S_{SO4}$ (Figure 8). The slope, however, varies greatly among the different sites
614 (Figure 8). In general, the sites from the shallower estuary environments have a more
615 moderate slope (0.35-0.44), meaning the sulfur isotopes increase rapidly relative to
616 the oxygen isotopes, while the shallow marine sediments have steeper slopes (0.99-
617 1.1), and the deep-sea sediments have the steepest slopes (1.7 and 1.4 respectively).
618 The ODP Sites thus show the fastest increase in the $\delta^{18}O_{SO4}$ relative to the $\delta^{34}S_{SO4}$
619 compared with the shallower sites. The changes in the slope among the different sites
620 correlates with the depth dependent sulfate concentration profiles, where the higher
621 the rate of change in the sulfate concentration with depth below the sediment-water
622 interface, the lower the slope, or the more quickly the sulfur isotopes evolve relative
623 to the oxygen isotopes. Site P130 (Mediterranean) is the exception and does not show
624 a linear relationship between $\delta^{18}O_{SO4}$ and $\delta^{34}S_{SO4}$, likely due to poor sampling
625 resolution.

626 Previous studies have shown a similar initial linear relationship between
627 $\delta^{18}O_{SO4}$ and $\delta^{34}S_{SO4}$, with the slope ranging between 1:1.4 (=0.71 compared to our
628 cross plots, Aharon and Fu, 2000) to 1:4.4 (=0.22, Mandernack et al., 2003). Our data
629 (Figure 8) displays a wider variation in slope than previously reported, as anticipated
630 in this study. Most authors have attributed the linear evolution of sulfur versus
631 oxygen isotopes in sulfate during BSR to a fully kinetic isotope effect in a closed
632 system under 'Rayleigh distillation', neglecting equilibrium oxygen isotope
633 fractionation. The SALP, however, includes the equilibrium oxygen isotope effect
634 during initial BSR prior to reaching apparent equilibrium.

635 We calculated the net sulfate reduction rate (nSRR) from each site from a curve fit
636 of the sulfate concentration profiles in the pore fluids using the general diagenetic
637 equation (Berner, 1980). As sulfate from the ocean diffuses into the sediments to be
638 reduced to sulfide, the length, or depth, scale over which sulfate concentrations
639 decrease relates to the overall rate of sulfate reduction. We assume the sulfate
640 concentration is in steady state (this is based on the fact that the age of the sediments
641 at all the sites in this study is much higher than the characteristic timescale of
642 diffusion) and no advection. However, we acknowledge that these assumptions may
643 be wrong in some of our sites. To augment our data we also present nSRR from pore
644 fluids profiles in previously published studies, where sulfate concentrations and sulfur
645 and oxygen isotopes in sulfate were published. This allows us to scale our results and
646 model to an even wider range of environments than those we directly measured.
647 Table EA.1 in the electronic annex summarizes data from the literature and the
648 location for each site.

649 In this larger dataset, the inverse of the slope between $\delta^{18}O_{SO4}$ vs. $\delta^{34}S_{SO4}$ is
650 positively correlated with the logarithm of the nSRR (Figure 10). This observation
651 confirms the hypothesis of Böttcher at al. (1998, 1999), who suggested that increases
652 in overall nSRR, would result in decreases in the expressed sulfur and oxygen isotope
653 fractionation, and thus the shape of $\delta^{18}O_{SO4}$ vs. $\delta^{34}S_{SO4}$ in sedimentary pore fluids.

5.3 The Mechanism of BSR in marine sediments

654 Our compilation from pore fluids in a diverse range of natural environments
655 suggests a correlation between the SALP and the nSRR (Figure 10). This association
656 may provide further understanding about the mechanism of BSR in the natural

environment. Combining the first order approximation for the SALP (equation 7) together with equations 8, 9 and 10 yields:

$$SALP = \frac{1}{1 - X_1 \cdot X_3} \cdot \frac{\frac{\varepsilon^{18}O_{f\_1}}{X_1 \cdot X_3} + \frac{\varepsilon^{18}O_{f\_3}}{X_1} + \delta^{18}O_{H2O} + \varepsilon^{18}O_{exchange} - \delta^{18}O_{SO4(0)}}{\frac{\varepsilon^{34}S_{f\_1}}{X_1 \cdot X_3} + \frac{\varepsilon^{34}S_{f\_3}}{X_1} + \varepsilon^{34}S_4} \quad (11)$$

Equation 13 shows that the SALP is a function of both X_1 and X_3 and does not depend on one more than the other. Hence, a change in the SALP does not necessarily tell us which one of the above (X_1 or X_3) plays more important role in the relative evolution of $\delta^{18}O_{SO4}$ vs. $\delta^{34}S_{SO4}$.

In order to address the question of the relative importance of X1 vs. X3 in the natural environment, we solved Equation 5 for three different cases:

1) X_1 varies and X_3 is fixed (close to unity) – that is, the flow of sulfate in and out of the cell varies but the recycling of sulfite is fixed such that nearly all the sulfite is reoxidized back to the internal sulfate pool.

2) X_3 varies and X_1 is fixed (close to unity) – that is the percentage of the recycling of the sulfite varied but the flow of sulfate in and out of the cell is fixed such that nearly all the sulfate that is brought into the cell exit the cell eventually.

3) Both X_1 and X_3 vary simultaneously.

The initial condition for this calculation is set by the isotopic composition of surface seawater sulfate (roughly 10‰ and 20‰ for oxygen and sulfur isotopes, respectively). The kinetic sulfur isotope effect for each step is similar to the values previously described (Rees, 1973). The kinetic oxygen isotope fractionation is taken

679 to be 1/4 of the fractionation of the sulfur isotope (Mizutani and Rafter, 1969). The
680 total equilibrium oxygen isotope fractionation between sulfite and the AMP-sulfite
681 complex and ambient water is taken as 17‰, which produces an apparent equilibrium
682 of about 22 ‰ in the case where X_1 and X_3 equal 1 (Equation 8). As discussed in the
683 introduction, it is enigmatic what impact temperature has on the $\delta^{18}O_{SO4(A.E)}$. We
684 therefore consider equilibrium oxygen isotope fractionation between sulfite and the
685 AMP-sulfite complex and ambient water as constant among the different
686 environments (equation 8). The results from this calculation are shown in figure 11a-
687 11c, with the measured data included for comparison in figure 11d.

688 The model solution for $\delta^{18}O_{SO4}$ and $\delta^{34}S_{SO4}$, when varying X_3 only (Figure
689 11b) fits the general behavior of pore fluid sulfur and oxygen isotopes (Figure 11d)
690 highlighting the importance of X_3 on the relative evolution of $\delta^{18}O_{SO4}$ and $\delta^{34}S_{SO4}$ in
691 the natural environment. The best-fit curves for the pore fluids in this study are
692 presented as the solid lines in figure 11d. This calculation suggests values for X_1 near
693 unity (ranging between 0.96 to 0.99 -- indicating up to 99 % of the sulfate brought
694 into the cell is ultimately recycled back out the cell). However, we suggest that this
695 kind of forward modeling is not accurate enough to estimate the real values for X_1 and
696 X_3 in natural environments due to the uncertainty with the values in our model as well
697 as the application of a closed system model to pore fluids. Therefore, changes in X_1
698 may be more important to the relative evolution of $\delta^{18}O_{SO4}$ vs. $\delta^{34}S_{SO4}$ than our
699 calculation suggest. In addition, our solution is valid only if BSR is the only process
700 that affects sulfur and oxygen isotopes in sulfate – which may not be the case. Other
701 subsurface processes can also affect this evolution, such as pyrite oxidation (e.g. Balci
702 et al., 2007; Brunner, et al., 2008; Heidel and Tichomirowa, 2011; Kohl and Bao,

2011) or sulfur disproportionation (Cypionka et al., 1998; Böttcher et al., 2001; Böttcher and Thamdrup, 2001; Böttcher, 2005).

Although most of the sites with $\delta^{18}O_{SO4}$ and $\delta^{34}S_{SO4}$ data seem to fit our model, our closed system model cannot replicate scenarios where the apparent equilibrium values are relatively high (26-30 ‰) together with a steep SALP (higher than ~1) in the uppermost sediments. As a result, by applying the closed system model, we cannot simulate data from Sites like ODP Site 1225 (Blake et al., 2006; Böttcher et al., 2006) and ODP Site 1130 (Wortmann et al., 2007). We suggest that this may be an artifact of the uncertainty in the values of the oxygen isotopic fractionation during various intracellular processes or erroneous model assumptions; these include the possible importance of temperature on oxygen exchange with ambient water (e.g. Fritz et al, 1989; Zeebe, 2010) or our assumption that this isotope exchange is complete, which it may not be (Brunner et al., 2012). The high sulfur isotope fractionation (>40‰) at these sites is consistent with the occurrence other complicating factors, such as activation of the trithionite pathway or subsurface sulfur disproportionation (Canfield and Thamdrup, 1994; Brunner and Bernasconi, 2005) that may skew the SALP, but which our model does not take into account.

5.4 The role of sulfite reoxidation in marine sediments

Our model suggests that X_3 varies between 0.4 and ~1 in the natural environments we studied (Figure 11), and is inversely correlated with nSRR. This hints that the reduction of sulfite to sulfide (Step 4) is connected to nSRR in marine sediments and may be the "bottleneck reaction", or significant branching point, for overall BSR. The faster the reduction of sulfite to sulfide, and therefore faster overall SRR, less

726 sulfite is being reoxidaized back to the outer sulfate pool. But what environmental or
727 natural parameters control the functioning of this bottleneck?

728 We attribute secondary importance to pressure differences (also Vossmeyer et al.,
729 2012) among natural environments, since we found similar isotope behavior among
730 sites that varied in water depth (i.e. pressure). Similar to Kaplan and Rittenberg
731 (1963) and Bradley et al. (2011), we speculate that one of the major environmental
732 factors that could impact the different behavior of the communities of sulfate reducing
733 bacteria might be related to the supply of the electron from the electron donor or
734 carbon source. It has been shown that the nature and concentration of different
735 electron donors is connected to the dynamics of each step during BSR (Detmers et al.,
736 2001; Bruchert 2004; Sim et al., 2011b), and the overall nSRR (e.g. Westrich and
737 Berner, 1984). Our data suggest that the higher the nSRR, the lower the sulfite
738 reoxidation (over step 4, sulfite reduction). This recycling of sulfite likely plays a
739 critical role during BSR in marine sediments. One possibility is that where the
740 availability of the electron donor is low (less organic matter availability), such as in
741 deep marine sediments, sulfate reducing bacteria might maintain high intracellular
742 concentrations of sulfite, which is manifest geochemically as the rapid change in
743 $\delta^{18}O_{SO4}$ relative to the slower change in $\delta^{34}S_{SO4}$. This could be contrasted with
744 environments where there is high organic matter availability (for example marginal
745 and shallow marine environments) where significant concentrations of intracellular
746 sulfite would be unnecessary. Although highly speculative, we suggest there is a
747 relationship between the concentration of intracellular sulfite and the availability of
748 the electron donor in the natural environment. Our data suggests that this relationship
749 may impact the relative fluxes within the bacterial sulfate reducing community.

Although this paper deals specifically with BSR in the marine environment, it is likely that our results are applicable to BSR in other systems including freshwater and groundwater systems. In these environments the hydrology is much more poorly constrained and the effects of advection and dispersion must be considered (Knoller et al., 2007). While we have taken the first steps towards expanding the applicability of this isotope approach to resolving mechanism, the next logical steps would be to extend the approach to the terrestrial environment where BSR can play a critical role in water quality.

6. SUMMARY AND CONCLUSIONS

In this study we presented pore fluid measurements of $\delta^{34}S_{SO4}$ and $\delta^{18}O_{SO4}$ from seven new sites spanning a shallow estuary to a deep-sea sediment. These pore fluid profiles exhibited behavior similar to previously published pore fluid profiles; the $\delta^{34}S_{SO4}$ increases monotonically during bacterial sulfate reduction, while the $\delta^{18}O_{SO4}$ increased and at some point levels off, when it has reached apparent equilibrium. When we plot the $\delta^{34}S_{SO4}$ vs $\delta^{18}O_{SO4}$ in this large range of natural environments we explored the reason behind the change in slope of $\delta^{34}S_{SO4}$ vs $\delta^{18}O_{SO4}$. Combining our results with literature data, we demonstrated that the slope of this line correlated to the net sulfate reduction rate, as has been suggested in previous studies. At sites with high sulfate reduction rates, the $\delta^{18}O_{SO4}$ increases more slowly relative to the $\delta^{34}S_{SO4}$, where at sites with lower sulfate reduction rates, the $\delta^{18}O_{SO4}$ increases more quickly relative to the $\delta^{34}S_{SO4}$. We reformulated the widely used model for the relative evolution of sulfur and oxygen isotopes in sulfate during BSR.

We used this new model with our data to explore how the intracellular fluxes impact the evolution of $\delta^{18}O_{SO4}$ vs. $\delta^{34}S_{SO4}$ during bacterial sulfate reduction.

Our new data, together with our new model, suggested that the most significant factor controlling the evolution of $\delta^{18}O_{SO4}$ vs. $\delta^{34}S_{SO4}$ in the natural environment is the ratio between the fluxes of intracellular sulfite oxidation and APS reduction (X_3). The variation in the ratio and its correlation to the nSRR implies that sulfite reduction may be the bottleneck reaction during BSR. We suggested that this recycling allows sulfate reduction to proceed even when the organic matter availability is low.

7. FIGURE CAPTIONS

Figure 1: The steps of bacterial sulfate reduction and the potential of oxygen and sulfur isotopic fractionations. i_{j_j}, $^{34}S_{i\_j}$ and $^{18}O_{i\_j}$ are the flux and the fractionation effect for sulfur and oxygen, respectively, for the forward (i=f) and backward (i=b) reaction j (j=1...4). X_k (k=1,2 and 3) is the ratio between the backward and forward fluxes.

Figure 2: Schematic possible behavior of sulfate during bacterial sulfate reduction as SO_4^{-2}, $\delta^{18}O_{SO4}$ and $\delta^{34}S_{SO4}$ profiles (a) and $\delta^{18}O_{SO4}$ vs. $\delta^{34}S_{SO4}$ (b). 'Trend A' shows

789 that $\delta^{18}O_{SO4}$ and $\delta^{34}S_{SO4}$ increase at a constant ratio, while sulfate reduction propagates
790 with depth (e.g. Aharon and Fu, 2000). 'Trend B' shows an increase in $\delta^{34}S_{SO4}$ and
791 $\delta^{18}O_{SO4}$ values at the onset of the curve, $\delta^{18}O_{SO4}$ reaches equilibrium values as sulfate
792 reduction prorogates with depth while $\delta^{34}S_{SO4}$ continue to increase.

793 Figure 3: Simplification of the bacterial sulfate reduction pathway shown in figure 1
794 without the APS intermediate, and considering two branching points (Farquhar et al,
795 2003; Canfield et al, 2006).

796

797 Figure 4: θ_O vs. $^{34}S_{total}$ diagram as calculated by equations 9 and 10. The gray circles
798 are calculated from Mangalo et al. (2008). The numbers are the values of nitrate
799 concentrations in the corresponding experiment. Error bars are calculated by the error
800 between two parallel growth experiments.

801

802 Figure 5: The SALP vs. nitrite concentration (a) and X_1 (grey squares) and X_3 (black
803 squares) vs. the SALP from pure culture *D.desulfuricans* (modified after Mangalo et
804 al. 2008) (b). Error bars for the SALP are calculated by the difference between two
805 parallel growth experiments, and the error bars for X_1 and X_3 indicate the maximum
806 and minimum values calculated using equations 9 and 10. The lines in panel b are the
807 best-fit curves of the linear regression.

808

809

810 Figure 6: Maps of the study area in a map of the world (a), and a map of the Eastern
811 Mediterranean region (b). The dots and the corresponding labels indicate the site
812 locations and names, respectively.

Figure 7: Pore fluid profiles in the Yarqon estuary at sites Y1 (filled symbols) and Y2 (open symbols) of SO_4^{2-} (a), $\delta^{18}O_{SO4}$ (b), and $\delta^{34}S_{SO4}$ (c). Pore fluid profiles in the Mediterranean Sea at sites HU (filled symbols), BA1 (gray symbols) and P130 (open symbols) of SO_4^{2-} (d), $\delta^{18}O_{SO4}$ (e) and $\delta^{34}S_{SO4}$ (f). Pore fluid profiles in ODP Sites 807 (filled symbols) and 1052 (open symbols) of SO_4^{2-} (g), $\delta^{18}O_{SO4}$ (h) and $\delta^{34}S_{SO4}$ (i).

Figure 8: $\delta^{18}O_{SO4}$ vs. $\delta^{34}S_{SO4}$ data in pore fluid sulfate of all studied sites. The lines are the linear regressions for Sites Y1, HU and 807.

Figure 9: The SALP and function of X_3 (where X_1 is fixed and close to unity) for 3 different scenarios: Closed system (according to equation 13), simulation of typical deep-sea sediment and simulation of typical estuary sediment.

Figure 10: The slope of $\delta^{34}S_{SO4}$ vs. $\delta^{18}O_{SO4}$ in the apparent linear phase of BSR vs. the average nSRR, as deduced from our data and worldwide pore fluid profiles. Data are presented from this study (open circles) and from other references (close circles). The labels of each point indicate the site's name (the coresponding references for each site are given in Table EA.1 in the electronic annex).

Figure 11: Schematic $\delta^{18}O_{SO4}$ vs. $\delta^{34}S_{SO4}$ plots, where X_1 varies and X_3 is fixed (close to unity) (a), X_3 varies and X_1 is fixed (close to unity) (b), both X_1 and X_3 vary simultaneously (c) and $\delta^{18}O_{SO4}$ vs. $\delta^{34}S_{SO4}$ data of pore fluid sulfate, the solid lines are the best-fit solution for X_1 and X_3 for each site as the color of the line is corresponding

838 to the calculated X_3 value (d). [(a)] This study [(b)]Ahron and Fu (2000), [(c)]Turchyn et al.
839 (2006).

840

841 **8. REFERENCES**

842

843 Aharon P. and Fu B. (2000) Microbial sulfate reduction rates and sulfur and oxygen
844 isotope fractionations at oil and gas seeps in deepwater Gulf of Mexico.
845 *Geochim. Cosmochim. Acta* **64**(2), 233–246.

846 Aharon P. and Fu B. (2003) Sulfur and oxygen isotopes of coeval sulfate–sulfide in
847 pore fluids of cold seep sediments with sharp redox gradients. *Chem. Geol.*
848 **195**, 201-218.

849 Aller R. C. and Blair N. E. (1996) Sulfur diagenesis and burial on the Amazon Shelf:
850 major control by physical sedimentation processes. *Geol-Mar. Lett.* **16**, 3–10.

851 Aller R. C., Madrid V., Chistoserdov A., Aller J. Y. and Heilbrun C. (2010) Unsteady
852 diagenetic processes and sulfur biogeochemistry in tropical deltaic muds:
853 Implications for oceanic isotope cycles and the sedimentary record. *Geochim.*
854 *Cosmochim. Acta* **74**, 4671-4692.

855 Balci N., Shanks W., Bernhard M. and Mandernack K. (2007) Oxygen and sulfur
856 isotope systematics of sulfate produced by bacterial and abiotic oxidation of
857 pyrite. *Geochim. Chosmochim. Acta* **71**, 3796–3811.

858 Berner R. A. (1980) *Early diagenesis: A theoretical approach.* Princeton Univ Pr.

859 Betts R. H. and Voss R. H. (1970) The kinetics of oxygen exchange between the
860 sulfite ion and water. *Can. J. Chem*. **48**, 2035–2041.

Blake, R. E., Surkov, A. V., Böttcher, M. E., Ferdelman, T. G. and Jørgensen, B. B. (2006) Oxygen isotope composition of dissolved sulfate in deep-sea sediments: Eastern Equatorial Pacific Ocean. In Proceedings of the Ocean Drilling Programm, Scientific Results, vol. 201 (eds. B. B. Jørgensen, S. L. D'Hondt and D. J. Miller). ODP, pp. 1–24.

Booth, I. R. (1985) Regulation of cytoplasmic pH in bacteria. *Microbiol. Rev.* **49**, 359–378.

Böttcher M. E. and Thamdrup B. (2001) Anaerobic sulfide oxidation and stable isotope fractionation associated with bacterial sulfur disproportionation in the presence of MnO_2. *Geochim. Cosmochim. Acta.* **65**, 1573–1581.

Böttcher, M.E., Brumsack, H.J., and de Lange, G.J., (1998) Sulfate reduction and related stable isotope (^{34}S, ^{18}O) variations in interstitial waters from the eastern Mediterranean. *In* (Eds. Robertson, A.H.F., Emeis, K.-C., Richter, C., and Camerlenghi, A.), *Proc. ODP, Sci. Results,* **160**: College Station, TX (Ocean Drilling Program), 365–373.

Böttcher M. E., Bernasconi S. M. and Brumsack H.J. (1999) Carbon, sulfur, and oxygen isotope geochemistry of interstitial waters from the western Mediterranean. In *Proceedings of the Ocean Drilling Program, Scientific Results*, vol. 161 (eds. R. Zahn, M. C. Comas and A. Klaus), pp. 413–421. Proceedings of the Ocean Drilling Program, Scientific Results. Ocean Drilling Program, College Station, TX.

Böttcher M. E., Thamdrup B. and Vennemann T. W. (2001) Oxygen and sulfur isotope fractionation during anaerobic bacterial disproportionation of elemental sulfur. *Geochim. Cosmochim. Acta* **65**, 1601–1609.

885 Böttcher M. E., Thamdrup B., Gehre M. and Theune A. (2005) $^{34}S/^{32}S$ and $^{18}O/^{16}O$
886 Fractionation during sulfur disproportionation by *Desulfobulbus propionicus*.
887 *Geomicrobiology Journal* **22**, 219.
888 Böttcher M. E., Ferdelman T. G., Jørgensen B. B., Blake R. E., Surkov A. V. and
889 Claypool G. E. (2006) Sulfur isotope fractionation by the deep biosphere
890 within sediments of the Eastern Equatorial Pacific and Peru Margin. In
891 *Proceedings of the Ocean Drilling Program, Scientific Result,s* Vol. **201 (**eds.
892 B.B. Jørgensen, S.L. D'Hondt and D.J. Miller). ODP, p.p 1-21.
893 Bradley A.S., Leavitt W. D. AND Johnston D. T. (2011). Revisiting the dissimilatory
894 sulfate reduction pathway. *Geobiology* **9**, 446–457.
895 Brüchert V. (2004) Physiological and ecological aspects of sulfur isotope
896 fractionation during bacterial sulfate reduction. In *Sulfur Biogeochemistry –*
897 *Past and Present,* vol. **379** (eds. J. P. Amend, K. J. Edwards and T. W. Lyons),
898 pp. 1–16. Geological Society of America Special Paper. Geological Society of
899 America, Boulder CO, USA.
900 Brüchert V., Knoblauch C. and Jørgensen B. B. (2001) Microbial controls on the
901 stable sulfur isotopic fractionation during bacterial sulfate reduction in Arctic
902 sediments. *Geochim. Cosmochim. Acta* **65**, 753–766.
903 Brunner B. and Bernasconi S. M. (2005) A revised isotope fractionation model for
904 dissimilatory sulfate reducing in sulfate reducing bacteria. *Geochim.*
905 *Cosmochim. Acta* **69**, 4759–4771.
906 Brunner B., Bernasconi S. M., Kleikemper J. and Schroth M. J. (2005) A model for
907 oxygen and sulfur isotope fractionation in sulfate during bacterial sulfate
908 reduction processes. *Geochim. Cosmochim. Acta* **69**, 4773–4785.

909 Brunner B., Mielke R. E., Coleman M. (2006) Abiotic oxygen isotope equilibrium
910 fractionation between sulfite and water. American Geophysical Union, Fall
911 Meeting 2006, Eos Trans AGU 87, abstract No. V11C-0601.
912 Brunner B., Yu J.-Y., Mielke R., MacAskill J., Madzunkov S., McGenity T. and
913 Coleman M. (2008) Different isotope and chemical patterns of pyrite oxidation
914 related to lag and exponential growth phases of Acidithiobacillus ferrooxidans
915 reveal a microbial growth strategy. *Earth Planet. Sci. Lett.***270**, 63–72.
916 Brunner B., Einsiedl F., Arnold G. L., Müller I., Templer S., Bernasconi S. (2012)
917 The reversibility of dissimilatory sulphate reduction and the cell-internal
918 multistep reduction of sulphite to sulphide: insights from the oxygen isotope
919 composition of sulphate. *Isotopes in Environmental & Health Studies* **48**, 33-
920 54
921 Canfield, D.E., (2001a). Biogeochemistry of sulfur isotopes. In: Valley, J.W., Cole,
922 D.R. (Eds.), *Reviews in Mineralogy and Geochemistry*, vol. **43**. Mineralogical
923 Society of America, Blacksburg, VA, pp. 607–636.
924 Canfield D. E. (2001b) Isotope fractionation by natural populations of sulfate-
925 reducing bacteria. *Geochim. Cosmochim. Acta* **65**, 1117–1124.
926 Canfield D.E. and Thamdrup B. (1994), The production of 34S-depleted sulfide
927 during bacterial disproportionation of elemental sulfur. *Science*, **266** , pp.
928 1973–1975
929 Canfield D. E., Olesen C. A. and Cox R. P. (2006) Temperature and its control of
930 isotope fractionation by a sulfate-reducing bacterium. *Geochim. Cosmochim.*
931 *Acta* **70**, 548–561.

Chiba H. and Sakai H. (1985) Oxygen isotope exchange-rate between dissolved sulfate and water at hydrothermal temperatures. *Geochim. Cosmochim. Acta* **49**, 993–1000.

Cypionka H., Smock A., and Böttcher M. E. (1998) A combined pathway of sulfur compound disproportionation in *Desulfovibrio desulfuricans. FEMS Microbiol Lett.* **166**, 181–186.

D'Hondt S., Jørgensen B. B., Miller D. J., Batzke A., Blake R., Cragg B. A., Cypionka H., Dickens G. R., Ferdelman T., Hinrichs K., Holm N. G., Mitterer R., Spivack A., Wang G., Bekins B., Engelen B., Ford K., Gettemy G., Rutherford S. D., Sass H., Skilbeck C. G., Aiello I. W., Guèrin G., House C. H., Inagaki F., Meister P., Naehr T., Niitsuma S., Parkes R. J., Schippers A., Smith D. C., Teske A., Wiegel J., Padilla C. N. and Acosta J. L. S. (2004) Distributions of Microbial Activities in Deep Subseafloor Sediments. *Science* **306**, 2216-2221.

Donahue M. A., Werne J. P., Meile C. and Lyons T. W. (2008) Modeling sulfur isotope fractionation and differential diffusion during sulfate reduction in sediments of the Cariaco Basin. *Geochim. Cosmochim. Acta* **72**, 2287-2297.

Eckert T., Brunner B., Edwards E. A. and Wortmann U. G. (2011) Microbially mediated re-oxidation of sulfide during dissimilatory sulfate reduction by Desulfobacter latus. *Geochim. Cosmochim. Acta* **75**, 3469-3485.

Farquhar J., Johnston D. T., Wing B. A., Habicht K. S., Canfield D. E., Airieau S. and Thiemens M. H. (2003) Multiple sulphur isotopic interpretations of biosynthetic pathways: implications for biological signatures in the sulphur isotope record. *Geobiology* **1**, 27–36.

Farquhar J., Johnston D. T. and Wing B. A. (2007) Implications of conservation of mass effects on mass-dependent isotope fractionations: Influence of network

957 structure on sulfur isotope phase space of dissimilatory sulfate reduction.
958 *Geochim. Cosmochim. Acta* **71**, 5862–5875.
959 Farquhar J., Canfield D. E., Masterson A., Bao H. and Johnston D. (2008) Sulfur and
960 oxygen isotope study of sulfate reduction in experiments with natural
961 populations from F_llestrand, Denmark. *Geochim. Cosmochim. Acta* **72**,
962 2805–2821.
963 Fritz P., Basharmal G. M., Drimmie R. J., Ibsen J. and Qureshi R. M. (1989) Oxygen
964 isotope exchange between sulfate and water during bacterial reduction of
965 sulfate. *Chem. Geol*. **79**, 99–105.
966 Froelich P., Klinkhammer G., Bender M., Luedtke N., Heath G. R., Cullen D.,
967 Dauphin P., Hammond D., Hartman B. and Maynard V. (1979) Early
968 oxidation of organic matter in pelagic sediments of the eastern equatorial
969 Atlantic: suboxic diagenesis. *Geochim. Cosmochim. Acta* **43,** 1075-1090.
970 Greene E. A., Hubert C., Nemati M., Jenneman G. E. and Voordouw G. (2003) Nitrite
971 reductase activity of sulphatereducing bacteria prevents their inhibition by
972 nitrate-reducing,sulphide-oxidizing bacteria. *Environ. Microbiol*. **5**, 607–617.
973 Harrison A. G. and Thode H. G. (1958) Mechanism of the bacterial reduction of
974 sulphate from isotope fractionation studies. *Trans. Faraday Soc*. **53**, 84–92.
975 Habicht K. S., Gade M., Thamdrup B., Berg P. and Canfield D. E. (2002) Calibration
976 of sulphate levels in the Archean Ocean. *Science* **298**, 2372–2374.
977 Heidel C., Tichomirowa M. (2011) The isotopic composition of sulfate from
978 anaerobic and low oxygen pyrite oxidation experimenzs with ferric iron - New
979 insights into oxidation mechanisms. *Chem. Geol.* **281**, 305-316.
980 Holler T., Wegener G., Niemann H., Deusner C., Ferdelman T. G., Boetius A.,
981 Brunner B., Widdel F. (2011). Carbon and sulfur back flux during anaerobic

microbial oxidation of methane and coupled sulfate reduction. *Proc. Natl. Acad. Sci. U.S.A.* **108**, 1484- 1490.

Horner D. A. and Connick R. E. (2003) Kinetics of oxygen exchange between the two isomers of bisulfite ion, disulfite ion ($S_2O_5^{2-}$), and water as studied by oxygen-17 Nuclear Magnetic Resonance Spectroscopy. *Inorg. Chem*. **42**, 1884–1894.

Johnston D. T., Farquhar J. and Canfield D. E. (2007) Sulfur isotope insights into microbial sulfate reduction: when microbes meet model. *Geochim. Cosmochim. Acta* **71**, 3929–3947.

Jørgensen B. B. (1979) A theoretical model of the stable sulfur isotope distribution in marine sediments. *Geochim. Cosmochim. Acta* **43**, 363–374

Kaplan I. R. and Rittenberg S. C. (1963) Microbiological fractionation of sulphur isotopes. *J. Gen. Microbiol.* **34**, 195–212.

Kasten S. and Jørgensen B. B. (2000) Sulfate Reduction in Marine Sediments. in *Marine geochemistry (eds, H. D. Schulz and M. zabel). Springer, Berlin, pp.* 263-281**.**

Kobayashi K, Tachibana S, IshimotoM(1969) Intermediary formation of trithionate in sulfite reduction by a sulfate-reducing bacterium. *Journal of Biochemistry (Tokyo)* **65**, 155.

Kohl I. E. and Bao H. (2006) Does enzyme-catalyzed formation of sulfate complexes cause oxygen isotope exchange during dissimilatory microbial sulfate reduction? Eos Trans AGU 87, V11C-0599.

Kohl I.E. and Bao H. (2011) Triple-oxygen-isotope determination of molecular oxygen incorporation in sulfate produced during abiotic pyrite oxidation (pH = 2–11). *Geochim. Cosmochim. Acta* **75,** 1785-1798

1006 Kohl I.E., Asatryan R. and Bao H. (2012). No oxygen isotope exchange between
1007 water and APS–sulfate at surface temperature: Evidence from quantum
1008 chemical modeling and triple-oxygen isotope experiments. *Geochim.*
1009 *Cosmochim. Acta* **95**, 106-118

1010 Lloyd R. M. (1968) Oxygen isotope behavior in sulfate–water system. *J. Geophys.*
1011 *Res.* **73**, 6099–6110.

1012 Mandernack K., Krouse H. R. and Skei J. M. (2003) A stable sulfur and oxygen
1013 isotopic investigation of sulfur cycling in an anoxic marine basin, Framvaren
1014 Fjord, Norway. *Chem. Geol.* **195**, 181–200.

1015 Mangalo M., Meckenstock R. U., Stichler W. and Einsiedl F. (2007) Stable isotope
1016 fractionation during bacterial sulfate reduction is controlled by reoxidation of
1017 intermediates. *Geochim. Cosmochim. Acta* **71**, 4161–4171.

1018 Mangalo M., Einsiedl F., Meckenstock R. U. and Stichler W. (2008) Influence of the
1019 enzyme dissimilatory sulfite reductase on stable isotope fractionation during
1020 sulfate reduction. *Geochim. Cosmochim. Acta* **71**, 4161–4171.

1021 Mizutani Y. and Rafter T. A. (1969) Oxygen isotopic composition of sulphates—Part
1022 4; bacterial fractionation of oxygen isotopes in the reduction of sulphates and
1023 in the oxidation of sulphur. *N. Z. J. Sci.* **12**, 60–68.

1024 Mizutani Y. and Rafter T. A. (1973) Isotopic behavior of sulphate oxygen in the
1025 bacterial reduction of sulphate. *Geochem. J.* **6**, 183–191.

1026 Niewöhner C., Hensen C., Kasten S., Zabel M. and Schulz H. D. (1998) Deep Sulfate
1027 Reduction Completely Mediated by Anaerobic Methane Oxidation in
1028 Sediments of the Upwelling Area off Namibia. *Geochim. Cosmochim. Acta*
1029 **62,** 455-464.

1030 Reeburgh W.S (2007) Oceanic Methane Biogeochemistry. *Chem. Rev.* **107**, pp 486–
1031 513.

1032 Rees C. E. (1973) A steady-state model for sulphur isotope fractionation in bacterial
1033 reduction processes. *Geochim. Cosmochim. Acta* **37**, 1141–1162.

1034 Sim M. S., Bosak T. and Ono S. (2011a) Large Sulfur Isotope Fractionation Does Not
1035 Require Disproportionation. *Science* **333,** 74-77.

1036 Sim M. S., Ono S., Donovan K., Templer S. P. and Bosak T. (2011b) Effect of
1037 electron donors on the fractionation of sulfur isotopes by a marine
1038 Desulfovibrio sp. *Geochim. Cosmochim. Acta* **75,** 4244-4259.

1039 Stam M. C., Mason P. R. D., Laverman A. M., Pallud C. and Cappellen P. V. (2011)
1040 $^{34}S/^{32}S$ fractionation by sulfate-reducing microbial communities in estuarine
1041 sediments. *Geochim. Cosmochim. Acta* **75,** 3903-3914.

1042 Tapgaar I. H., Røy H. and Jørgensen B. B. (2011) Concurrent low- and high-affinity
1043 sulfate reduction kinetics in marine sediment. *Geochim. Cosmochim. Acta* **75,**
1044 2997-3010.

1045 Turchyn A.V., Sivan O. and Schrag D. (2006) Oxygen isotopic composition of sulfate
1046 in deep sea pore fluid: evidence for rapid sulfur cycling. *Geobiology* **4,** 191-
1047 201

1048 Turchyn A.V., Brüchert V., Lyons T. W., Engel G. S., Balci N., Schrag D. P. and
1049 Brunner B. (2010) Kinetic oxygen isotope effects during dissimilatory sulfate
1050 reduction: A combined theoretical and experimental approach. *Geochim.*
1051 *Cosmochim. Acta* **74,** 2011-2024.

1052 Vossmeyer, A., Deusner C., Kato C., Inagaki F. and Ferdelman T.G. (2012) Substrate
1053 specific pressure-dependence of microbial sulfate reduction in deep-sea cold
1054 seep sediments of the Japan Trench. *Frontiers Microbiol*., **3**, 253

Westrich J.T and Berner R.B (1984) The role of sedimentary organic matter in bacterial sulfate reduction: The *G* model tested. *Limnol.Oceanogr*. **29**, 236-249.

Wortmann U. G., Bernasconi S. M. and Böttcher M. E. (2001) Hypersulfidic deep biosphere indicates extreme sulfur isotope fractionation during single-step microbial sulfate reduction. *Geology* **29**, 647–650.

Wortmann U. G. (2006) A 300 m long depth profile of metabolic activity of sulfate reducing bacteria in the continental margin sediments of South Australia (ODP Site 1130) derived from inverse reaction-transport modeling. G^3 **7**, Q05012.

Wortmann U. G., Chernyavsky B., Bernasconi S. M., Brunner B., Böttcher M. E. and Swart P. K. (2007) Oxygen isotope biogeochemistry of pore water sulfate in the deep biosphere: dominance of isotope exchange reactions with ambient water during microbial sulfate reduction (ODP Site 1130). *Geochim. Cosmochim. Acta* **71**, 4221–4232.

Wortmann U. G. and Chernyavsky B. M. (2011) The significance of isotope specific diffusion coefficients for reaction-transport models of sulfate reduction in marine sediments. *Geochim. Cosmochim. Acta* **75**, 3046-3056.

Zak I., Sakai H. and Kaplan I. R. (1980) Factors controlling the 18O/16O and 34S/32S isotope ratios of ocean sulfates, evaporates and interstitial sulfates from modern deep sea sediments. In *Isotope Marine Chemistry*. Institute of Geophysics and Planetary Physics, University of California Los Angeles, California 90024, USA, pp. 339–373 (Chapter 17).

1078 Zeebe R. E. (2010) A new value for the stable oxygen isotope fractionation between
1079 dissolved sulfate ion and water. *Geochimica et Cosmochimica Acta* **74**, 818–
1080 828.

ELECTRONIC ANNEX

Table EA. 1: Worldwide pore fluid SALP $^{-1}$, average nSRR (mol·cm^{-3}·year^{-1}) and the coresponding references

Site name	Location	S.A.L.P^{-1}	R^2	N[a]	nSRR	Temperature (°C)	References
Y1	Yarqon Stream estuary	2.3	0.998	11	$3\cdot10^{-5}$	28	This study
Y2	Yarqon Stream estuary	2.9	0.985	7	$1\cdot10^{-5}$	28	This study
HU	Eastern Mediterranean	1.0	0.979	9	$7\cdot10^{-8}$	20	This study
BA1	Eastern Mediterranean	0.9	0.983	10	$6\cdot10^{-8}$	14	This study
ODP 1052	NW Atlantic	0.6	0.989	8	$3\cdot10^{-12}$	2	This study
ODP 807	NW Pacific	0.7	0.953	15	$9\cdot10^{-13}$	2	This study
Gas	Gulf of Mexico	3.4	0.951	12	$5\cdot10^{-4}$ [b]	6	Aharon and Fu, (2000)
Oil	Gulf of Mexico	2.8	0.940	13	$3\cdot10^{-5}$ [b]	6	Aharon and Fu, (2000)
Ref	Gulf of Mexico	1.4	0.901	6	$2\cdot10^{-6}$ [b]	6	Aharon and Fu, (2000)
OST 2	Amazon delta	1.2	0.922	5	$7\cdot10^{-6}$ [c]	27	Aller et al., (2010)
ODP 1123	SW Pacific	0.9	0.914	8	$8\cdot10^{-12}$ [b]	2	Turchyn et al., (2006)
ODP 1086	West Africa	0.1	0.997	3	$1\cdot10^{-11}$ [b]	2	Turchyn et al., (2006)

(a) The number of analyses that were used for the liner regression.

(b) Calculated by the authors.

(c) Taken from Aller et al. (1996).

1081

EQUATIONS- GCA 8261

1082

1083

1084

Equation 1:

$$\varepsilon^{34}S_{total} = \varepsilon^{34}S_{f\_1} + X_1 \cdot \left(\varepsilon^{34}S_{f\_2} - \varepsilon^{34}S_{b\_1}\right) + \ldots$$
$$X_1 \cdot X_2 \cdot \left(\varepsilon^{34}S_{f\_3} - \varepsilon^{34}S_{b\_2}\right) + X_1 \cdot X_2 \cdot X_3 \cdot \left(\varepsilon^{34}S_{f\_4} - \varepsilon^{34}S_{b\_3}\right) \quad (1)$$

1085

1086

1087

Equation 2:

$$\varepsilon^{34}S_{total} = -3‰ + X_1 \cdot X_2 \cdot 25‰ + X_1 \cdot X_2 \cdot X_3 \cdot 25‰ \quad (2)$$

1088

1089

1090

Equation 3:

1091

$$\varepsilon^{18}O_{total} = \varepsilon^{18}O_{f\_1} + X_1 \cdot \left(\varepsilon^{18}O_{f\_2} - \varepsilon^{18}O_{b\_1}\right) + \ldots$$
$$X_1 \cdot X_2 \cdot \left(\varepsilon^{18}O_{f\_3} - \varepsilon^{18}O_{b\_2}\right) + X_1 \cdot X_2 \cdot X_3 \cdot \left(\varepsilon^{18}O_{f\_4} - \varepsilon^{18}O_{b\_3}\right) \quad (3)$$

1092

1093

Equation 4:

1094

$$\delta^{18}O_{SO4(A.E)} = \delta^{18}O_{H2O} + \varepsilon^{18}O_{exchange} + \frac{1}{X_3} \cdot \varepsilon^{18}O_{f\_3} \quad (4)$$

1095

1096

Equation 5:

1097

$$\delta^{18}O_{SO4(t)} = \begin{cases} \frac{\varepsilon^{18}O_{total}}{\varepsilon^{34}S_{total}} \cdot \left(\delta^{34}S_{SO4(t)} - \delta^{34}S_{SO4(0)}\right) + \delta^{18}O_{SO4(0)} & X_1 \cdot X_2 \cdot X_3 = 0 \\ \delta^{18}O_{SO4(A.E)} - \exp\left(-\theta_O \cdot \frac{\delta^{34}S_{SO4(t)} - \delta^{34}S_{SO4(0)}}{\varepsilon^{34}S_{total}}\right) \cdot \left(\delta^{18}O_{SO4(A.E)} - \delta^{18}O_{SO4(0)}\right) & 0 < X_1 \cdot X_2 \cdot X_3 < 1 \end{cases} \quad (5)$$

1098

Equation 6:

1099
$$\delta^{18}O_{SO4(t)} = \delta^{18}O_{SO4(0)} + \left(\delta^{18}O_{SO4(A.E)} - \delta^{18}O_{SO4(0)}\right) \cdot \theta_O \cdot \frac{\delta^{34}S_{SO4(t)} - \delta^{34}S_{SO4(0)}}{\varepsilon^{34}S_{total}} \quad (6)$$

1100

1101

Equation 7:

1102
$$SALP = \theta_O \cdot \frac{\delta^{18}O_{SO4(A.E)} - \delta^{18}O_{SO4(0)}}{\varepsilon^{34}S_{total}} \quad (7)$$

1103

Equation 8:

1104
$$\delta^{18}O_{SO4(A.E)} = \delta^{18}O_{H2O} + \varepsilon^{18}O_{exchange} + \frac{\varepsilon^{18}O_{f\_1}}{X_1 \cdot X_3} + \frac{\varepsilon^{18}O_{f\_3}}{X_3} \quad (8)$$

1105

1106

Equation 9:

1107
$$\theta_O = \frac{X_1 \cdot X_3}{1 - X_1 \cdot X_3} \quad (9)$$

1108

1109

Equation 10:

1110

$$\varepsilon^{34}S_{total} = -3 + 25 \cdot X_1 + 25 \cdot X_1 \cdot X_3 \quad (10)$$

1111

1112

1113

Equation 11:

1114

$$SALP = \frac{1}{1 - X_1 \cdot X_3} \cdot \frac{\frac{\varepsilon^{18}O_{f\_1}}{X_1 \cdot X_3} + \frac{\varepsilon^{18}O_{f\_3}}{X_1} + \delta^{18}O_{H2O} + \varepsilon^{18}O_{exchange} - \delta^{18}O_{SO4(0)}}{\frac{\varepsilon^{34}S_{f\_1}}{X_1 \cdot X_3} + \frac{\varepsilon^{34}S_{f\_3}}{X_1} + \varepsilon^{34}S_4} \quad (11)$$

1115

FIGURES

Figure 1:

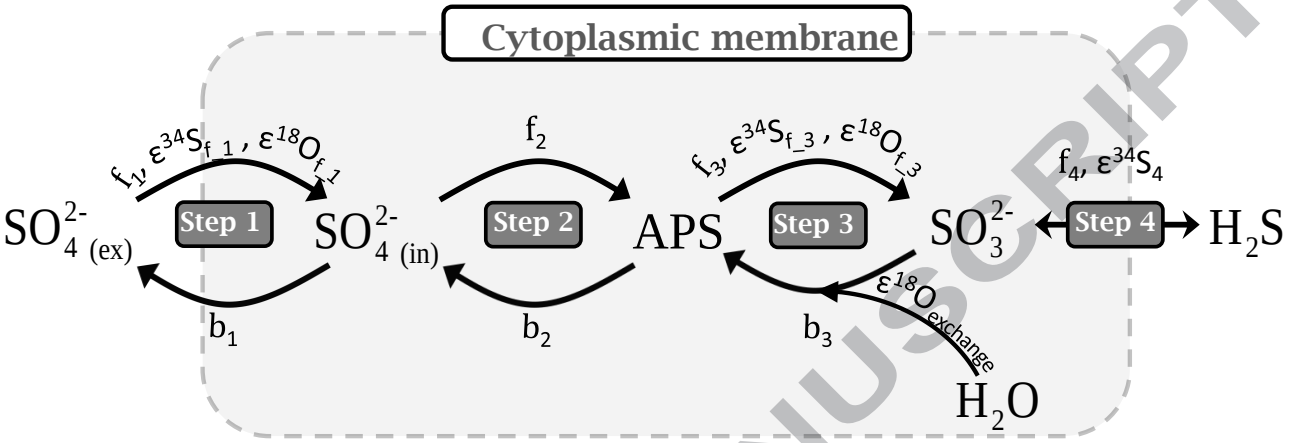

$$X_1 = \frac{b_1}{f_1} \qquad X_2 = \frac{b_2}{f_2} \qquad X_3 = \frac{b_3}{f_3}$$

Figure 2:

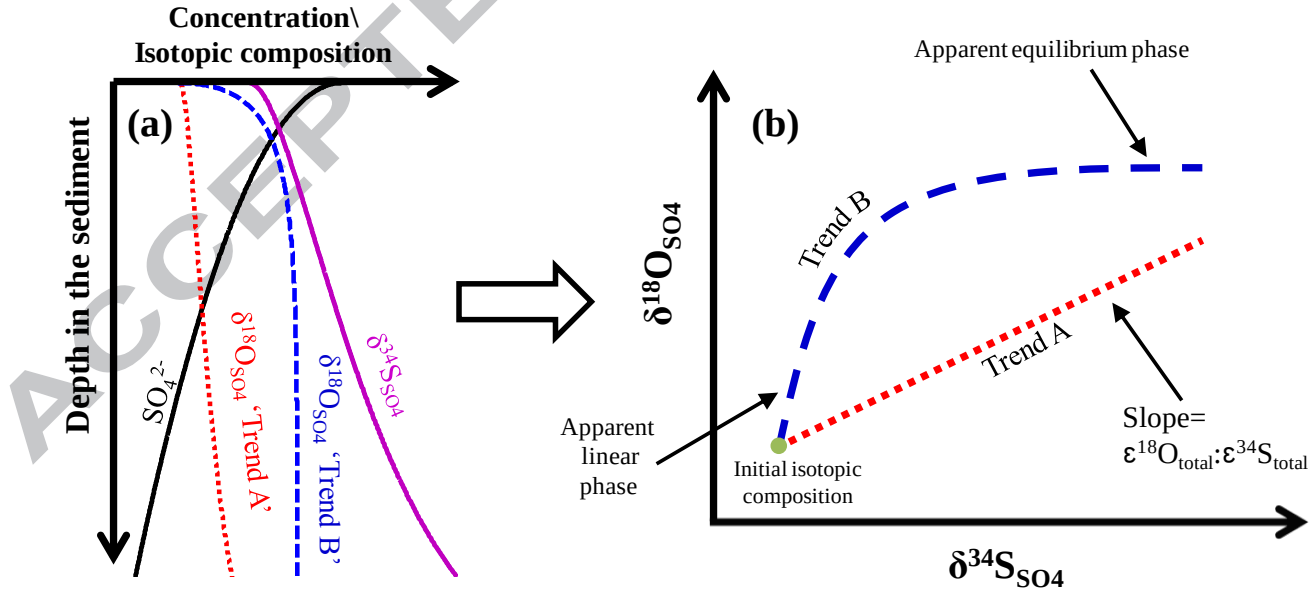

Figure 3:

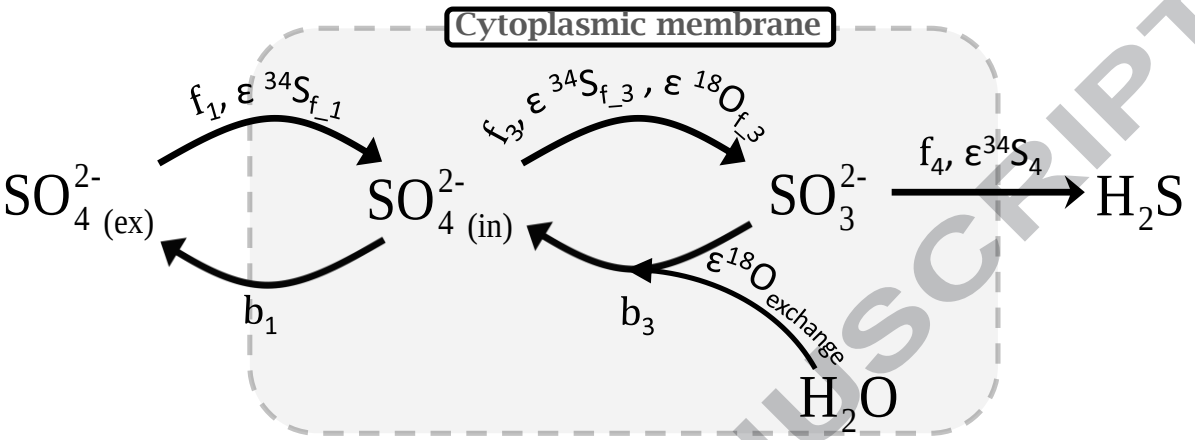

Figure 4:

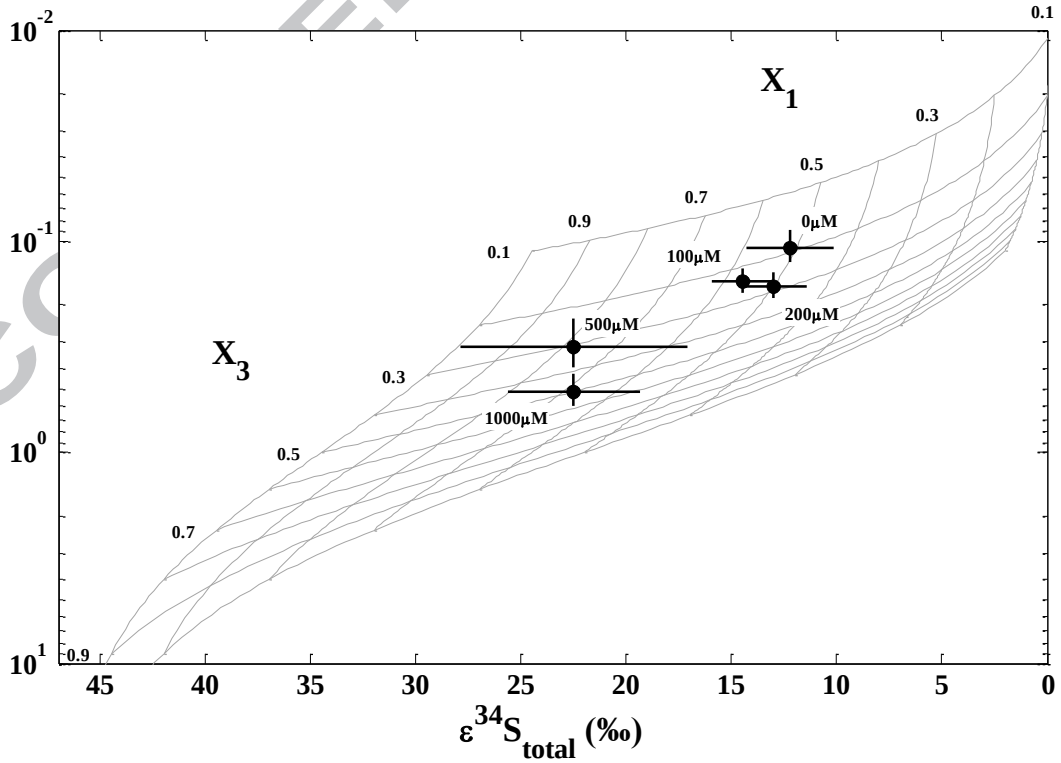

Figure 5:

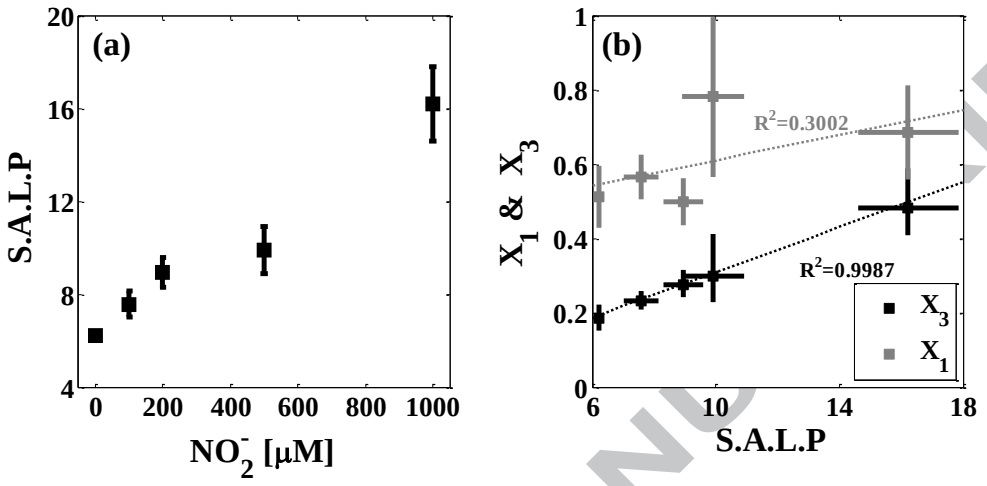

Figure 6:

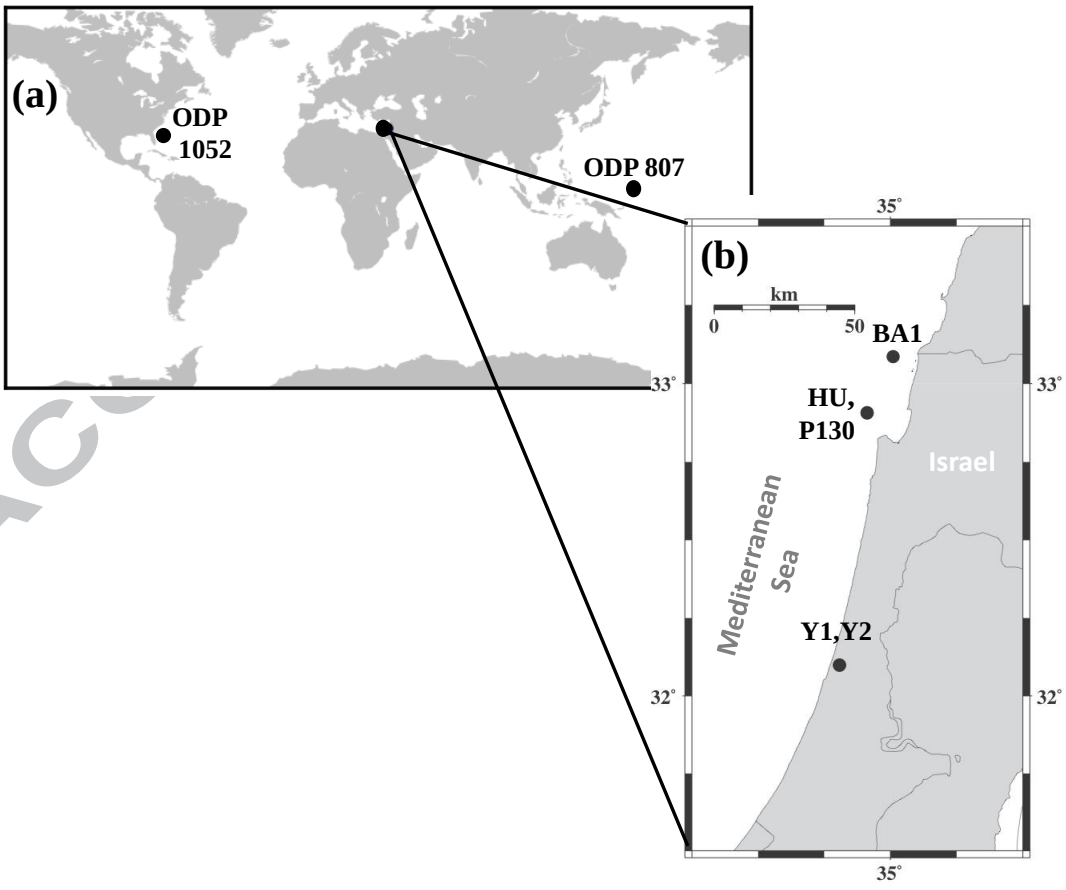

Figure 7:

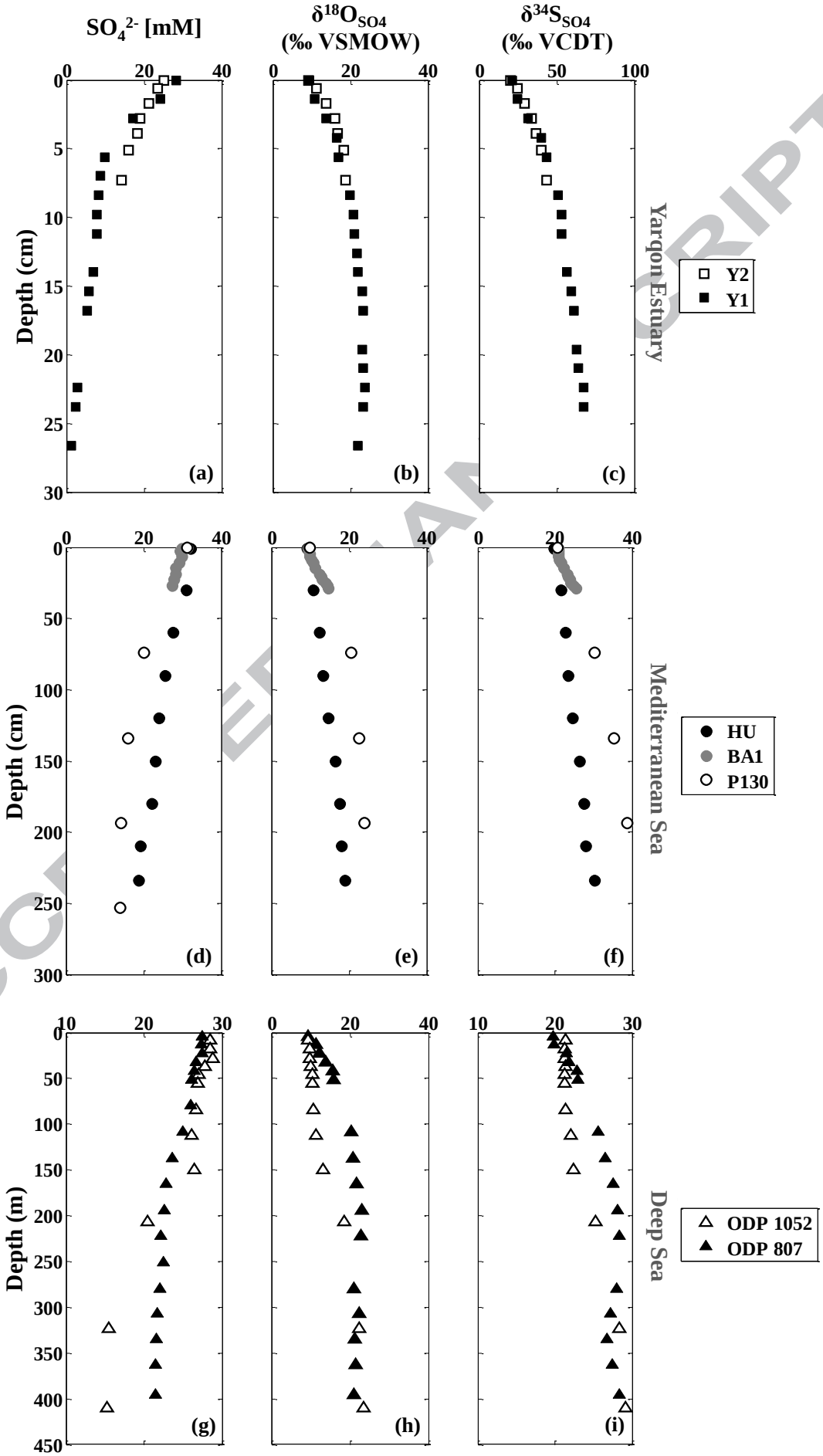

Figure 8:

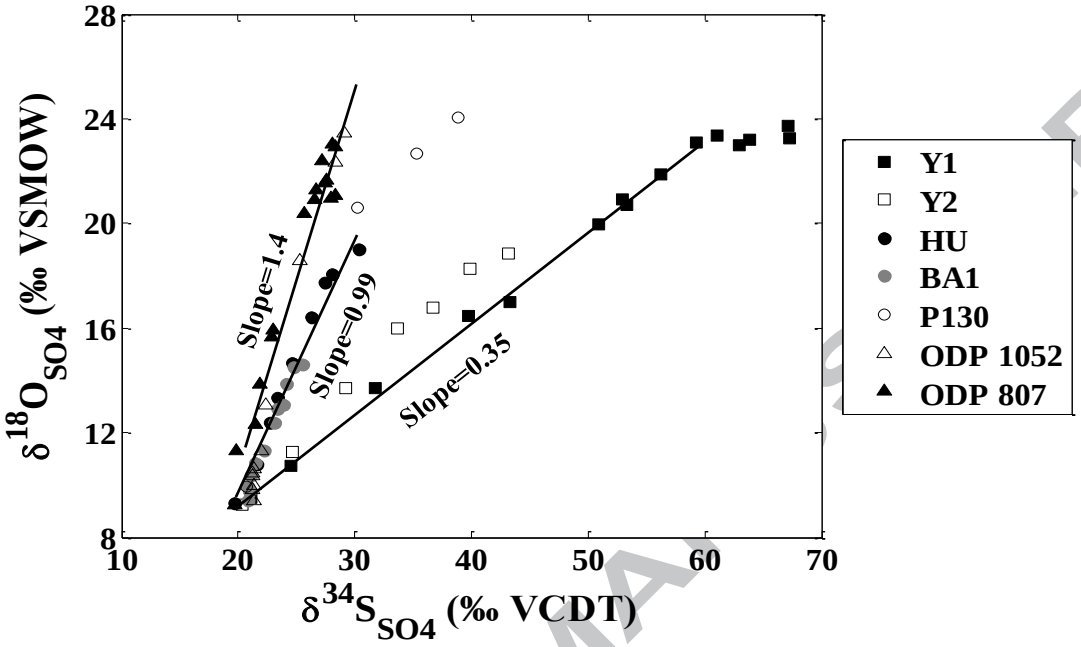

Figure 9:

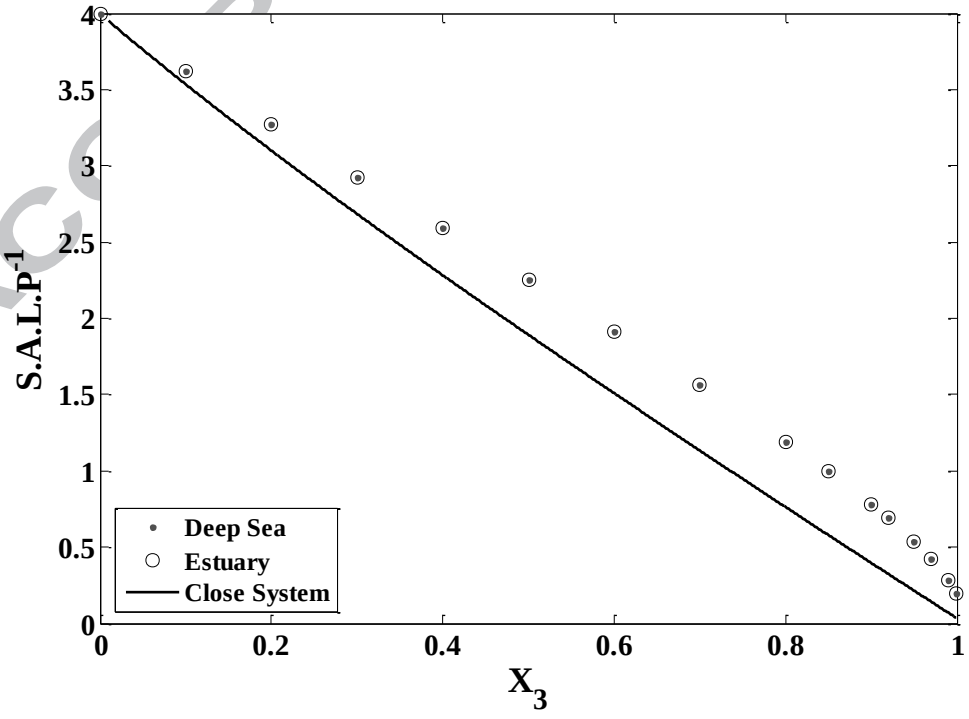

Figure 10:

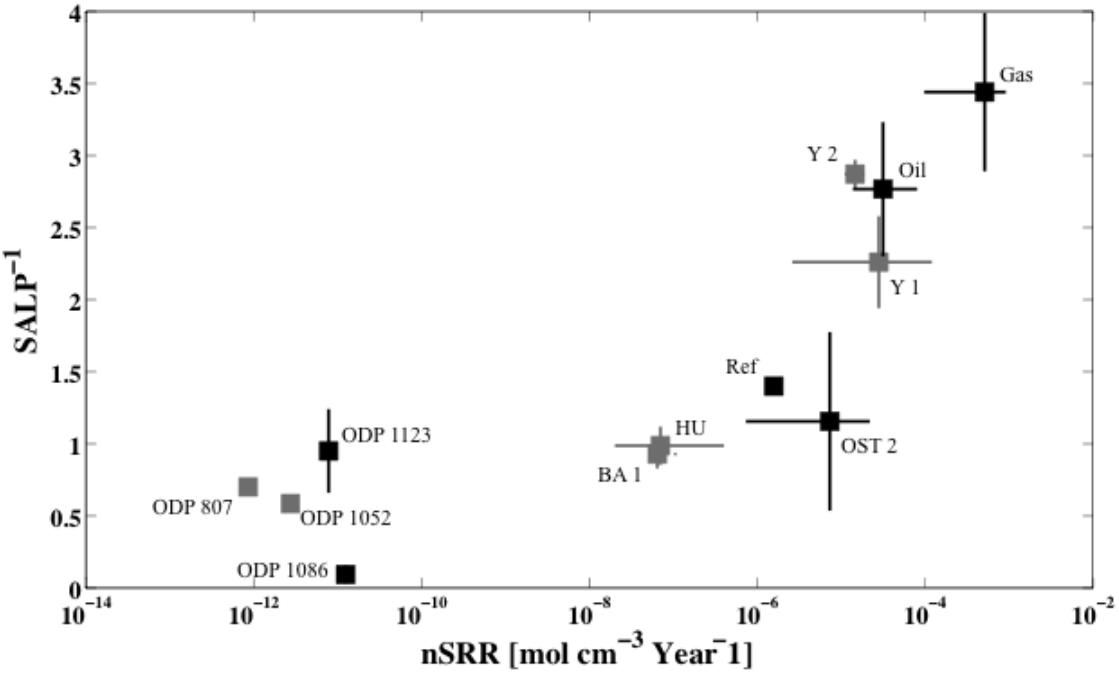

Figure 11: